Mass-transport for surface water waves

Hege G. Frøysa

Master Thesis in Applied and Computational Mathematics,
Department of Mathematics,
University of Bergen,
June 2021

Abstract

In this thesis we study the mass-transport and mean-water level for various waves. By expanding linear wave theory up to second order , we study the mass-transport for wave groups in deep and shallow water. Numerical experiments show that this expansion causes a negative mean water level. This has a great influence on the mass-transport in shallow water. However, for deep water this effect is negligible. We also calculate the mass-transport for shoaling waves using experimental data from a wave flume. As the water gets too shallow for linear theory to be valid, non-linear theory has to be applied. Finally, we compare particle paths and mean-water level from field measurements with theory. By using the KdV-equation, the theory explains the measurements well. A strong correlation between mass-transport and mean-water level is also observed.

Acknowledgments

First of all, I would like to thank my supervisor Henrik Kalisch. I'm grateful that you introduced me to the study of waves and gave me the opportunity to come along on your field experiments. Your help and enthusiasm has been highly valued! To my co-supervisor Maria Bjørnestad, thank you for always taking the time to help me. You have been a great support this year and made studying oranges even more fun.

To my fellow students, I'm thankful that you have created a study environment where people are always willing to help and discuss the problems faced. Thank you for making these five past years so great and for being encouraging when math made me cry. I would also like to thank the administration at the department for being so friendly and helping me out with whatever needed!

Lastly, I would like to thank my family for always cheering on me. Staying motivated throughout this year was a lot easier because of you and your support means a lot to me!

Contents

Introduction and thesis outline

As a wave propagates, the fluid particles experience a net transport. This transport is called the Stokes drift and was first described around 170 years ago [9, 21]. The magnitude of the transport is largest at the surface and decays with depth [11]. This established theory concerns waves where the mean water level equals zero, meaning the wave is centred around the equilibrium level. However, this is not always true. Low-frequency waves called infra-gravity waves can be induced by wave-groups of higher frequency. It was first observed by Munk in 1948 [16] and two years later Tucker found a positive correlation between the wave height of the wave group and the infra-gravity wave [20]. The infra-gravity wave propagate with the same velocity as the wave group and are therefore called bound infra-gravity waves [1]. The trough is aligned with the wave group's crest. This causes a negative mean-water level for the highest waves. By using second order wave theory, we want to understand how the mean water level changes the Stokes drift. This was done for wave groups with different wave lengths in both shallow and deep water. This method contains uncertainty as the velocity potential is not uniquely defined [12]. A similar study of the mass transport was done by Bremer and Taylor in 2016 where they calculated the Lagrangian trajectories for wave groups at different depths [22]. Several wave flume experiments regarding mass-transport have been done over the years. Measuring mass-transport in a closed wave flume is hard because the total mass-transport obviously has to be zero. Hence, there is disagreement as to what actually happens [21].

To understand more about the mass-transport and mean water level we have also studied what happens to shoaling waves. As a wave approaches a sloping beach, it gets steeper and the wave height increases [17]. Before the wave breaks, the mean water level is lowered [13]. This was confirmed in a wave flume experiment done by Bowen *et al.* in 1968 [4]. In this thesis we are not going into breaking waves. By using data from recent field experiments near the surf zone [2], we are also trying to find a theory modelling the measured particle trajectories and mean water levels.

Thesis outline

Chapter 1: The thesis starts out with some basic wave theory [11]. This theory is based on the Euler equation and conservation of mass. By adding boundary conditions to the fluid we are able to define the free surface problem. By linearizing, the problem is solved exactly. The Stokes drift is also defined.

Chapter 2: Linear wave theory is expanded up to second order using Longuet-Higgins' article [12]. For a wave group, the second order effect creates a low-frequency wave, often called the infra-gravity wave. We are running numerical experiments calculating the Stokes drift for wave groups consisting of different wave lengths.

Chapter 3: Based on the boundary conditions already defined, we derive the KdV-equation and it's periodic wave solution called the "cnoidal wave".

Chapter 4: The mass-transport for shoaling waves using linear and non-linear theory is compared to experimental data from [4]. This chapter is written like an article and will be submitted.

Chapter 5: In this chapter we present field experiments measuring the mean-water level and particle paths. The linear and non-linear theory derived in the earlier chapters are used to compare theoretical particle paths with the measured.

Chapter 6: The main results from the thesis are summarized and concludes the work.

Chapter 1

Wave Theory

In this chapter we are going to derive the free surface problem and can be found in Chapter 13 of [23]. We are then linearizing theory and finding the Stokes drift. This is found in Chapter 8 of [11].

When water waves are generated, take for example wind blowing on the ocean making a wave, gravity is mostly the restoring force. They are called interface waves and travel most often on the air-water interface. Other waves like internal waves or compression and expansion waves are not explained in this thesis. Our coordinate system is two-dimensional where x is the horizontal direction and z the vertical. The depth is given by h and η is the free surface. The velocity field is defined as $\mathbf{u}(x, z, t) = (u, w)$, where u is the horizontal velocity and w is the vertical. The parameters used to define a wave are the amplitude a, the spatial frequency k, also called wave number, and the circular frequency ω. The wave length λ is the distance from wave crest to crest and is defined as $\lambda = \frac{2\pi}{k}$. The period is denoted T and could also be defined as $T = \frac{2\pi}{\omega}$. The wave travels with phase speed $c = \frac{\omega}{k}$. Note that later in the thesis we use the wave height H. This is the distance from crest to trough, whereas the amplitude a is the distance from the still water line to the crest.

We start out with the continuity equation

$$\frac{\partial \rho}{\partial t} + \nabla \cdot (\rho \mathbf{u}) = 0 \tag{1.1}$$

which states the principle of conservation of mass. We are only concerned about

incompressible flow with constant density ρ, meaning the equation reduces to

$$\nabla \cdot \mathbf{u} = 0. \tag{1.2}$$

The other equation describing describing a fluid is the Navier-Stokes momentum equation. For incompressible and inviscid flow it is reduced to

$$\frac{D\mathbf{u}}{Dt} = \frac{\partial \mathbf{u}}{\partial t} + \mathbf{u} \cdot \nabla \mathbf{u} = -\frac{\nabla p}{\rho} + \mathbf{g} \tag{1.3}$$

and named the Euler equation, which is a simplification of the Navier-Stokes momentum equation.
Lastly, we assume $\omega = \nabla \times \mathbf{u} = 0$, meaning the flow is irrotational. This makes it possible to define a velocity potential ϕ:

$$\mathbf{u} = \nabla \phi. \tag{1.4}$$

Substituting the velocity potential into (1.2) leads to the Laplace's equation

$$\Delta \phi = 0. \tag{1.5}$$

The free surface problem has three boundary conditions. Two of the are kinematic boundary conditions and the last one is dynamic. The first one says that water can't go trough the bottom. This means that the normal velocity there has to zero:

$$w = \partial \phi / \partial z = 0 \text{ on } z = -h. \tag{1.6}$$

The second boundary condition says that the fluid particles at the free surface must have the same normal velocity as the normal velocity of the surface itself. This means that the fluid particles that make up the interface can't leave the free surface and is written mathematically as

$$(\mathbf{n} \cdot \mathbf{u})_{z=\eta} = \mathbf{n} \cdot \mathbf{u_s} \tag{1.7}$$

where $\mathbf{n}$ is the surface normal and $\mathbf{u_s}$ is the velocity of the free surface. The surface can be defined as $f(x, z, t) = z - \eta(x, t) = 0$. The normal surface is then defined as $\mathbf{n} = \nabla f$ and using (1.7) leads to

$$\Big(- u\frac{\partial \eta}{\partial x} + w \Big)_{z=\eta} = \frac{\partial \eta}{\partial t}. \tag{1.8}$$

The boundary condition can also be written in terms of the velocity potential:

$$\Big(- \frac{\partial \phi}{\partial x}\frac{\partial \eta}{\partial x} + \frac{\partial \phi}{\partial z} \Big)_{z=\eta} = \frac{\partial \eta}{\partial t}. \tag{1.9}$$

It is assumed that the surface has a purely vertical velocity $\mathbf{u_s} = \partial\eta/\partial t\mathbf{e_z}$.

For the last boundary condition we need to re-write the Euler equation (1.3), into the Bernoulli equation:

$$\frac{\partial\phi}{\partial t} + \frac{1}{2}|\nabla\phi|^2 + \frac{p}{\rho} + gz = 0. \tag{1.10}$$

This is possible because the flow is irrotational, inviscid and incompressible. By saying that the pressure p just below the surface is the same pressure as p_0 just above, the Bernoulli equation is reduced to

$$\Big(\frac{\partial\phi}{\partial t} + \frac{1}{2}|\nabla\phi|^2 + gz\Big)_{z=\eta} = 0. \tag{1.11}$$

and we have the last boundary condition called the dynamic boundary conditions.

To summarize, the partial derivatives are written in a more compact form and the free surface problem then looks like:

$$\begin{aligned} \phi_{xx} + \phi_{zz} &= 0 & \\ \phi_z &= 0 & \text{on } z = -h \\ \eta_t + \phi_x\eta_x - \phi_z &= 0 & \text{on } z = \eta \\ \phi_t + \frac{1}{2}(\phi_x^2 + \phi_z^2) + g\eta &= 0 & \text{on } z = \eta \end{aligned} \tag{1.12}$$

1.1 Linear Theory

For waves with small amplitudes and slopes the problem can be linearized. The goal is to solve for the velocity potential ϕ. It is assumed that the components u, w and η are all of the same order and higher order terms will then be neglected.

The kinematic boundary condition (1.8) simplifies to

$$\Big(\frac{\partial \phi}{\partial z}\Big)_{z=\eta} = \frac{\partial \eta}{\partial t}. \tag{1.13}$$

The left hand side is expanded around $z = 0$ leading to

$$\Big(\frac{\partial \phi}{\partial z}\Big)_{z=\eta} = \Big(\frac{\partial \phi}{\partial z}\Big)_{z=0} + \eta\Big(\frac{\partial^2 \phi}{\partial z^2}\Big)_{z=0} + ... \approx \frac{\partial \eta}{\partial t} \tag{1.14}$$

where the higher order terms are neglected and we are left with the linearized form of the kinematic boundary condition:

$$\Big(\frac{\partial \phi}{\partial z}\Big)_{z=0} = \frac{\partial \eta}{\partial t}. \tag{1.15}$$

The dynamic boundary condition (1.11) is simplified by dropping the non-linear terms and expanding around $z = 0$. The linear condition then looks like this

$$\Big(\frac{\partial \phi}{\partial t}\Big)_{z=0} + g\eta = 0. \tag{1.16}$$

Since the free surface problem now is defined for the linear case, the velocity potential ϕ can be found. We assume that the wave takes the shape:

$$\eta(x,t) = a\,\cos\big(kx - \omega t\big). \tag{1.17}$$

Looking at the boundary conditions we see that the solution needs to be a sine function of phase $(kx - \omega t)$ for η to be correct. Therefore a solution is "guessed" in the form of

$$\phi(x,z,t) = f(z)\,\sin(kx - \omega t) \tag{1.18}$$

where $f(z)$ needs to be found. Substituting (1.18) into (1.5) leads to

$$\frac{d^2 f}{dz^2} - k^2 f = 0 \tag{1.19}$$

which has the solution $f(z) = Ae^{kz} + Be^{-kz}$ where A and B are constants. The velocity potential becomes

$$\phi(x, z, t) = (Ae^{kz} + Be^{-kz}) \sin(kx - \omega t). \tag{1.20}$$

The constants are found by substituting (1.20) into the no flow trough condition (1.6):

$$k(Ae^{-kh} - Be^{kh}) \sin(kx - \omega t) = 0 \implies B = Ae^{-2kh} \tag{1.21}$$

and using the kinematic boundary condition gives

$$k(A - B) \sin(kx - \omega t) = \omega a \sin(kx - \omega t) \implies k(A - B) = \omega a. \tag{1.22}$$

The constants are then found to be

$$A = \frac{a\omega}{k(1 - e^{-2kh})} \quad \text{and} \quad B = \frac{a\omega e^{-2kh}}{k(1 - e^{-2kh})} \tag{1.23}$$

and the velocity potential can then finally be defined as

$$\phi(x, z, t) = \frac{a\omega}{k} \frac{\cosh(k(z + h))}{\sinh(kh)} \sin(kx - \omega t). \tag{1.24}$$

The velocities in the x and z-direction then easy to find:

$$u = \frac{\partial \phi}{\partial x} = a\omega \frac{\cosh(k(z + h))}{\sinh(kh)} \cos(kx - \omega t) \tag{1.25}$$

$$w = \frac{\partial \phi}{\partial z} = a\omega \frac{\sinh(k(z + h))}{\sinh(kh)} \sin(kx - \omega t). \tag{1.26}$$

Until now, the dynamic boundary condition has not been used. Inserting ϕ and η into (1.11) produces

$$-\frac{a\omega^2}{k} \frac{\cosh(kh)}{\sinh(kh)} \cos(kx - \omega t) = -ga \cos(kx - \omega t) \tag{1.27}$$

which simplifies to what is called the dispersion relation:

$$\omega = \sqrt{gk \tanh(kh)}. \tag{1.28}$$

The dispersion relation explains how the temporal and spatial frequency are connected. Since the phase speed of the waves is given by $c = \omega/k$ it can by using this relation be written

$$c = \sqrt{\frac{g}{k} \tanh(kh)} = \sqrt{\frac{g\lambda}{2\pi} \tanh\left(\frac{2\pi h}{\lambda}\right)}. \tag{1.29}$$

Waves with larger wavelength λ will then travel faster compared to shorter waves.

1.2 Stokes Drift

For the linearized particle paths, the motion is closed circles or ellipses. The mean velocity of a particle will then be zero. If something is thrown into the ocean, it will slowly drift in the direction of propagation. Thus the mean velocity is not zero and this slow movement is called Stokes drift. By keeping higher order terms in the Taylor series of the velocity of the particle

$$\frac{dx}{dt} = u(x,z,t) = u(x_0,z_0,t) + (x-x_0)\Big(\frac{\partial u}{\partial x}\Big)_{x_0,z_0} + (z-z_0)\Big(\frac{\partial u}{\partial z}\Big)_{x_0,z_0} + ... \quad (1.30)$$

$$\frac{dz}{dt} = w(x,z,t) = w(x_0,z_0,t) + (x-x_0)\Big(\frac{\partial w}{\partial x}\Big)_{x_0,z_0} + (z-z_0)\Big(\frac{\partial w}{\partial z}\Big)_{x_0,z_0} + ..., \quad (1.31)$$

the Stokes drift can be obtained. The position (x_0, z_0) is the fluid's location if there was no waves. The velocities are defined in (1.25) and (1.26). The horizontal and vertical distances in the Taylor series are defined like

$$x - x_0 = \int_0^t u(x_0,z_0,t')dt' \quad (1.32)$$

$$= -a\frac{\cosh(k(z_0+H))}{\sinh(kH)}\sin(kx_0-\omega t) \quad (1.33)$$

$$z - z_0 = \int_0^t w(x_0,z_0,t')dt' \quad (1.34)$$

$$= a\frac{\sinh(k(z_0+H))}{\sinh(kH)}\cos(kx_0+\omega t). \quad (1.35)$$

Integrating (1.30) and (1.31) over a period T and then dividing by T, the time averages are found:

$$\bar{u}_S = a^2\omega k\frac{\cosh(2k(z_0+h))}{2\sinh^2(kh)} \quad (1.36)$$

$$\bar{w}_S = 0\,. \quad (1.37)$$

As seen, there is no Stokes drift in the vertical direction. As the particles moves in the direction of wave propagation, it causes mass transport. Another word for Stokes drift is mass transport velocity. The Stokes drift is also the difference between Eulerian and Lagrangian velocity [21]:

$$\text{Stokes drift= Lagrangian - Eulerian} \quad (1.38)$$

Chapter 2

Second order wave theory

The derivations of the theory done in this chapter are based on Longuet-Higgins and Stewart's article "Radiation stress and mass transport in gravity waves, with application to 'surf beats' " [12].

2.1 The Stokes Approximation

An expansion of the variables $\mathbf{u}$, ϕ, η and p are made in the Stokes' method of approximation as

$$\begin{aligned} \mathbf{u} =& \mathbf{u}^{(1)} + \mathbf{u}^{(2)} + ... \\ \phi =& \phi^{(1)} + \phi^{(2)} + ... \\ \eta =& \eta^{(1)} + \eta^{(2)} + ... \\ p + \rho g z =& p^{(1)} + p^{(2)} + ... \end{aligned} \tag{2.1}$$

where the first terms, $\mathbf{u}^{(1)}$, $\phi^{(1)}$ etc., satisfy the first order equations and boundary conditions. Then $\mathbf{u}^{(1)} + \mathbf{u}^{(2)}$, $\phi^{(1)} + \phi^{(2)}$ etc. satisfy the equations and boundary conditions up to second order. The first order variables, like $\phi^{(1)}$, were found in Chapter 1. For this chapter we want to expand and define the problem up to second order.

The velocity potential $\phi^{(2)}$ is defined like

$$\begin{aligned}
\nabla^2\phi^{(2)} &= 0, \\
(\partial\phi^{(2)}/\partial z)_{z=-h} &= 0 \\
\left(\frac{\partial^2\phi^{(2)}}{\partial t^2} + g\frac{\partial\phi^{(2)}}{\partial z}\right)_{z=0} &= -\Big\{\frac{\partial}{\partial t}(\mathbf{u}^{(1)2}) + \eta^{(1)}\frac{\partial}{\partial z}\left(\frac{\partial^2\phi^{(1)}}{\partial t^2} + g\frac{\partial\phi^{(1)}}{\partial z}\right)\Big\}_{z=0}.
\end{aligned} \tag{2.2}$$

When $\phi^{(2)}$ is found, the rest of the variable $\mathbf{u}^{(2)}$, $p^{(2)}$ and $\eta^{(2)}$ may also be found through these equations:

$$\begin{aligned}
\mathbf{u}^{(2)} &= \nabla\phi^{(2)}, \\
p^{(2)}/\rho &= -(\frac{\partial\phi^{(2)}}{\partial t} + \frac{1}{2}\mathbf{u}^{(1)2}), \\
g\eta^{(2)} &= -\Big(\frac{\partial\phi^{(2)}}{\partial t} + \frac{1}{2}\mathbf{u}^{(1)2} + \eta^{(1)}\frac{\partial^2\phi^{(1)}}{\partial z\partial t}\Big)_{z=0}
\end{aligned} \tag{2.3}$$

For one single wave these equations can be solved relatively easy and the solution for $\phi^{(2)}$ is

$$\phi^{(2)} = \frac{3a^2\omega}{8\sinh^4 kh}\cosh\ 2k(z+h)\sin\ 2(kx-\omega t) + Cx + Dt. \tag{2.4}$$

For a group of waves, it is more difficult finding the solution. The next section will solve the problem for a wave group of two waves at uniform depth, but it is possible to expand to n waves.

2.2 Method for solving the second order theory

This method systematically uses the expansion method explained above. A wave group consisting of two waves is defined by

$$\eta^{(1)} = a_1\ \cos(k_1x - \omega_1 t) + a_2\ \cos(k_2x - \omega_2 t) \tag{2.5}$$

where a_n is the amplitude, k_n is the wave number and ω_n is the radian frequency. The frequency and wave number are related through the dispersion relation

$$\omega_n^2 = gk_n\ \tanh(k_nh). \tag{2.6}$$

The first-order potential corresponding to (2.5) is

$$\phi^{(1)} = \frac{a_1\omega_1\ \cosh\ k_1(z+h)}{k_1\sinh k_1h}\sin(k_1x-\omega_1t) + \frac{a_2\omega_2\ \cosh\ k_2(z+h)}{k_2\sinh k_2h}\sin(k_2x-\omega_2t). \tag{2.7}$$

To define the problem up to second-order, (2.2) is solved for $\phi^{(2)}$. The right hand side needs to be defined and the first step is to find $(\mathbf{u}^{(1)})^2$ evaluated in $z = 0$. This is written as

$$(\mathbf{u}^{(1)})^2 = u^2 + w^2 \,|_{z=0}. \tag{2.8}$$

First u^2 is calculated

$$u^2 = \left(\sum_{n=1}^{2} \frac{a_n \omega_n \, \cosh(k_n h)}{\sinh(k_n h)} \cos(k_n x - \omega_n t) \right)^2 \tag{2.9}$$

$$= \sum_{n,m=1}^{2} \frac{a_n a_m \omega_n \omega_m \, \cosh(k_n h) \cosh(k_m h)}{\sinh(k_n h) \sinh(k_m h)} \cos(k_n x - \omega_n t) \, \cos(k_m x - \omega_m t) \tag{2.10}$$

and then w^2

$$w^2 = \left(\sum_{n=1}^{2} a_n \omega_n \, \sin(k_n x - \omega_n t) \right)^2 \tag{2.11}$$

$$= \sum_{n,m=1}^{2} a_n a_m \omega_n \omega_m \, \sin(k_n x - \omega_n t) \, \sin(k_m x - \omega_m t). \tag{2.12}$$

Adding these together will give a summation in terms of $(k_n - k_m)$ and $(k_n + k_m)$. Then $\phi^{(2)}$ and $\eta^{(2)}$ are also going to contain these terms. The summation terms in the cosine-function will be neglected since only the averaged values over several wavelengths are of interest. Then

$$u^2 + w^2 = \sum_{n,m=1}^{2} \frac{a_n a_m \omega_n \omega_m}{\sinh(k_n h) \sinh(k_m h)} \Big[\cosh(k_n h) \cosh(k_m h) \, \cos(k_n x - \omega_n t) \cos(k_m x - \omega_m t) \tag{2.13}$$

$$+ \sinh(k_n h) \sinh(k_m h) \, \sin(k_n x - \omega_n t) \sin(k_m x - \omega_m t) \Big]$$

$$\overset{(*)}{=} \sum_{n,m=1}^{2} \frac{a_n a_m \omega_n \omega_m}{\sinh(k_n h) \sinh(k_m h)} \Big[\cosh(k_n h) \cosh(k_m h) \, \frac{\cos((k_n - k_m)x - (\omega_n - \omega_m)t)}{2}$$

$$+ \sinh(k_n h) \sinh(k_m h) \, \frac{\cos((k_n - k_m)x - (\omega_n - \omega_m)t)}{2} \Big]$$

$$\overset{(**)}{=} \sum_{n,m=1}^{2} \frac{a_n a_m \omega_n \omega_m \, \cosh((k_n + k_m)h)}{2 \, \sinh(k_n h) \sinh(k_m h)} \cos((k_n - k_m)x - (\omega_n - \omega_m)t) \tag{2.14}$$

where the identities

$$(*):\ \cos(\alpha)\cos(\beta) = \frac{\cos(\alpha-\beta)+\cos(\alpha+\beta)}{2} \tag{2.15}$$

$$\sin(\alpha)\sin(\beta) = \frac{\cos(\alpha-\beta)-\cos(\alpha+\beta)}{2} \tag{2.16}$$

$$(**):\ \cosh(\alpha+\beta) = \cosh(\alpha)\cosh(\beta)+\sinh(\alpha)\sinh(\beta) \tag{2.17}$$

are used. Writing $(k_n - k_m)$, $(\omega_n - \omega_m) = \Delta k$, $\Delta\omega$ finally gives:

$$(\mathbf{u}^{(1)})^2 = \sum_{n,m=1}^{2} \frac{a_n a_m \omega_n \omega_m \cosh((k_n+k_m)h)}{2\sinh(k_n h)\sinh(k_m h)} \cos(\Delta k x - \Delta\omega t) \tag{2.18}$$

Taking the time derivative of (2.18) and using averaged values k and ω to simplify gives

$$\frac{\partial}{\partial t}(\mathbf{u}^{(1)})^2 = \sum_{n,m=1}^{2} \frac{a_n a_m \omega^2 \cosh(2kh)}{2\sinh^2(kh)} \Delta\omega \sin(\Delta k x - \Delta\omega t) \tag{2.19}$$

Next, we have

$$\frac{\partial}{\partial z}\left(\frac{\partial^2}{\partial t^2} + g\frac{\partial}{\partial z}\right)\phi^{(1)}_{z=0} = \sum_{n=1}^{2} -a_n\omega_n^3 \sin(k_n x - \omega_n t) + \sum_{n=1}^{2} \frac{a_n\omega_n g k_n \cosh(k_n h)}{\sinh(k_n h)} \sin(k_n x - \omega_n t) \tag{2.20}$$

$$= \sum_{n=1}^{2} a_n\omega_n \sin(k_n x - \omega_n t)(-\omega_n^2 + \frac{g k_n}{\tanh(k_n h)}) \tag{2.21}$$

$$= \sum_{n=1}^{2} a_n\omega_n^3 \sin(k_n x - \omega_n t)(-1 + \frac{1}{\tanh^2(k_n h)}) \tag{2.22}$$

$$= \sum_{n=1}^{2} a_n\omega_n^3 \sin(k_n x - \omega_n t)(\frac{-\sinh^2(k_n h)}{\sinh^2(k_n h)} + \frac{\cosh^2(k_n h)}{\sinh^2(k_n h)}) \tag{2.23}$$

$$= \sum_{n=1}^{2} \frac{a_n\omega_n^3 \sin(k_n x - \omega_n t)}{\sinh^2(k_n h)}. \tag{2.24}$$

where the dispersion relation (2.6) is used. Thus

$$\eta^{(1)}\frac{\partial}{\partial z}\left(\frac{\partial^2}{\partial t^2} + g\frac{\partial}{\partial z}\right)\phi^{(1)}_{z=0} = \sum_{m=1}^{2} a_m \cos(k_m x - \omega_m t) \cdot \sum_{n=1}^{2} \frac{a_n\omega_n^3 \sin(k_n x - \omega_n t)}{\sinh^2(k_n h)}$$

$$\overset{(*)}{=} \sum_{n,m=1}^{2} \frac{a_n a_m \omega_m^3}{2\sinh^2(k_m h)} \sin(\Delta k x - \Delta\omega t) \tag{2.25}$$

where the identity

$$(*):\ \sin(\alpha)\cos(\beta) = \frac{\sin(\alpha+\beta)+\sin(\alpha-\beta)}{2} \tag{2.26}$$

is used and only the difference terms are kept. Splitting the equation up in two halves and reversing n and m for the second half makes the right-hand side of (2.25) look like:

$$\sum_{n,m=1}^{2} \frac{1}{2}\,\frac{a_n a_m \omega_n^3}{2\sinh^2(k_n h)}\sin(\Delta kx - \Delta\omega t) + \sum_{m,n=1}^{2} \frac{1}{2}\,\frac{a_n a_m \omega_m^3}{2\sinh^2(k_m h)}\sin(-\Delta kx + \Delta\omega t) \tag{2.27}$$

$$= \sum_{n,m=1}^{2} \frac{1}{2}\,\frac{a_n a_m \omega_n^3}{2\sinh^2(k_n h)}\sin(\Delta kx - \Delta\omega t) - \sum_{m,n=1}^{2} \frac{1}{2}\,\frac{a_n a_m \omega_m^3}{2\sinh^2(k_m h)}\sin(\Delta kx - \Delta\omega t) \tag{2.28}$$

$$= \sum_{n,m=1}^{2} \frac{a_n a_m}{4}\left(\frac{\omega_n^3}{\sinh^2 k_n h} - \frac{\omega_m^3}{\sinh^2 k_m h}\right)\sin(\Delta kx - \Delta\omega t) \tag{2.29}$$

Using Taylor's expansion to the first order, this can be written as

$$\sum_{n,m=1}^{2} \frac{a_n a_m}{4}\Delta\omega\frac{d}{d\omega}\left(\frac{\omega^3}{\sinh^2 kh}\right)\sin(\Delta kx - \Delta\omega t) \tag{2.30}$$

After all these calculations, (2.2) can be defined as

$$\left(\frac{\partial^2\phi^{(2)}}{\partial t^2} + g\frac{\partial\phi^{(2)}}{\partial z}\right)_{z=0} = -\sum_{n,m=1} (K a_m a_n \Delta\omega)\sin(\Delta kx - \Delta\omega t) \tag{2.31}$$

where

$$K = \frac{\omega^2\cosh 2kh}{2\sinh^2 kh} + \frac{1}{4}\frac{d}{d\omega}\left(\frac{\omega^3}{\sinh^2 kh}\right). \tag{2.32}$$

The solution of $\phi^{(2)}$ is

$$\phi^{(2)} = -K\sum_{n,m=1}^{2} \frac{a_m a_n c_g}{gh\theta - c_g^2}\,\frac{\cosh\Delta k(z+h)}{\cosh\Delta kh}\,\frac{\sin(\Delta kx - \Delta\omega t)}{\Delta k} \tag{2.33}$$

where

$$\theta = \frac{\tanh\Delta kh}{\Delta kh}. \tag{2.34}$$

It is worth mentioning that it is possible to add terms like $Cx + Dt$ to the velocity potential and the solution will still be correct. However, just to not

complicate things more, this is not done. From (2.33) it is easy to find the horizontal velocity component

$$u^{(2)} = \frac{\partial \phi^{(2)}}{\partial x} = -K \sum_{n,m=1}^{2} \frac{a_m a_n c_g}{gh\theta - c_g^2} \frac{\cosh(\Delta k(z+h))}{\cosh \Delta kh} \cos(\Delta kx - \Delta \omega t). \quad (2.35)$$

The second order equation for the free surface is defined by (2.3). Now we have all the variables needed and it is just to plug in:

$$\begin{aligned} g\eta^{(2)} =& - \Bigg[K \sum_{n,m=1}^{2} \frac{a_n a_m c_g^2}{gh\theta - c_g^2} \cos(\Delta kx - \Delta \omega t) + \sum_{n,m=1}^{2} \frac{1}{4} \frac{a_n a_m \omega^2 \cosh(2kh)}{sinh^2(kh)} \cos(\Delta kx - \Delta \omega t) \\ & - \sum_{n,m=1}^{2} \frac{a_n a_m \omega^2}{2} \cos(\Delta kx - \Delta \omega t) \Bigg] \\ =& - K \sum_{n,m=1}^{2} \frac{a_n a_m c_g^2}{gh\theta - c_g^2} \cos(\Delta kx - \Delta \omega t) + \sum_{n,m=1}^{2} \frac{1}{2} a_n a_m \omega^2 \cos(\Delta kx - \Delta \omega t)(-\frac{1}{2} \frac{\cosh(2kh)}{\sinh^2(kh)} + 1) \\ =& - K \sum_{n,m=1}^{2} \frac{a_n a_m c_g^2}{gh\theta - c_g^2} \cos(\Delta kx - \Delta \omega t) - \sum_{n,m=1}^{2} \frac{a_n a_m \omega^2}{4 \sinh^2(kh)} \cos(\Delta kx - \Delta \omega t). \end{aligned} \quad (2.36)$$

The final calculation is to rewrite the constant K. Since $k = k(\omega)$, the calculation is a bit lengthy and some steps are skipped. Hence

$$\begin{aligned} K =& \frac{\omega^2 \cosh(2kh)}{2 \sinh^2(kh)} + \frac{1}{4} \left[\frac{3\omega^2}{\sinh^2(kh)} + \frac{d}{dk} \left(\frac{\omega^3}{\sinh^2(kh)} \right) \frac{\partial k}{\partial \omega} \right] \\ =& \frac{\omega^2 \cosh(2kh)}{2 \sinh^2(kh)} + \frac{1}{4} \left[\frac{3\omega^2}{\sinh^2(kh)} + \frac{d}{dk} \left(\frac{\omega^3}{\sinh^2(kh)} \right) \frac{1}{\frac{\partial \omega}{\partial k}} \right] \\ =& (...) = \frac{\omega^2}{4 \sinh^2(kh)} \frac{\sinh(4kh) + 3\sinh(2kh) + 2kh}{\sinh(2kh) + 2kh} \end{aligned} \quad (2.37)$$

and the wave problem up to second order is now defined.

In Figure 2.1, we have plotted $\eta^{(1)}$ and $\eta^{(2)}$ for a arbitrary wave group. The second order effect is called the bounded infra-gravity wave as it propagates with the wave group. The crest of the wave group is where the trough of the infra-gravity wave is, causing a negative mean water level.

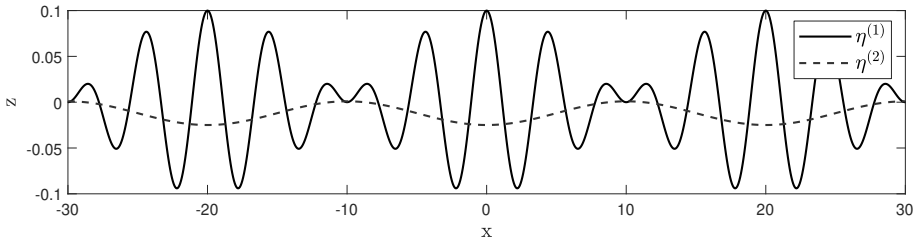

Figure 2.1: The free surface of a wave group where the first and second order are plotted separately.

2.2.1 Stokes Drift

To find the Stokes drift, the exactly same procedure as for 1.2 is followed with the Taylor approximation:

$$u(x,z,t) = u(x_0,z_0,t) + (x-x_0)\frac{\partial u}{\partial x}\bigg|_{x_0,z_0} + (z-z_0)\frac{\partial u}{\partial z}\bigg|_{x_0,z_0} \tag{2.38}$$

The only difference in the calculation is that there are more terms. The horizontal velocity up to second order for a wave-group consisting of two waves is defined as

$$\begin{aligned} u(x,z,t) = &\frac{a_1\omega_1\cosh(k_1(z+h))}{\sinh(k_1h)}\cos(k_1x-\omega_1t) \\ &+ \frac{a_2\omega_2\cosh(k_2(z+h))}{\sinh(k_2h)}\cos(k_2x-\omega_2t) \end{aligned} \tag{2.39}$$

$$- Kc_g\Big[\frac{a_1^2+a_2^2}{gh-c_g^2} + \frac{2a_1a_2}{gh\theta-c_g^2}\frac{\cosh\Delta k(z+h)}{\cosh\Delta kh}\cos(\Delta kx-\Delta\omega t)\Big]. \tag{2.40}$$

The velocity is divided into two parts, (2.39) and (2.40), where the Stokes drift is calculated for each one and then added together. For (2.39), it is just to use the Stokes drift formula found in (1.36):

$$\bar{u}_S = a^2\omega_1k_1\frac{\cosh\ 2k_1(z_0+h)}{2\ \sinh^2 k_1h} + a^2\omega_2k_2\frac{\cosh\ 2k_2(z_0+h)}{2\ \sinh^2 k_2h}. \tag{2.41}$$

Then the next step is to find the Taylor approximation of (2.40). The horizontal

distance looks like

$$x - x_0 = \int_0^t u(x_0, z_0, t')dt' \tag{2.42}$$

$$= \int_0^t -Kc_g\Big[\frac{a_1^2 + a_2^2}{gh - c_g^2} + \frac{2a_1a_2}{gh\theta - c_g^2}\frac{\cosh\Delta k(z_0+h)}{\cosh\Delta kh}\cos(\Delta kx_0 - \Delta\omega t')\Big]dt' \tag{2.43}$$

$$= -Kc_g\Big[\frac{a_1^2 + a_2^2}{gh - c_g^2}t + \frac{2a_1a_2}{gh\theta - c_g^2}\frac{\cosh\Delta k(z_0+h)}{\cosh\Delta kh}\frac{\sin(\Delta kx_0 - \Delta\omega t)}{\Delta k}\Big] \tag{2.44}$$

It is noticed that $\mathcal{O}(a^4)$ will be obtained in the first order Taylor approximation (assuming that $\mathcal{O}(a_1) \sim \mathcal{O}(a_2)$). Since the amplitudes are small, it will be neglected. We are then left with the terms of $\mathcal{O}(a^2)$. After time-averaging we obtain

$$\bar{u}_S = -Kc_g\frac{a_1^2 + a_2^2}{gh - c_g^2} + \mathcal{O}(a^4) \tag{2.45}$$

and the total Stokes drift is then

$$\bar{u}_S = a_1^2\omega_1k_1\frac{\cosh(2k_1(z_0+h))}{2\sinh^2(k_1h)} + a_2^2\omega_2k_2\frac{\cosh(2k_2(z_0+h))}{2\sinh^2(k_2h)} \tag{2.46}$$

$$-Kc_g\frac{a_1^2 + a_2^2}{gh - c_g^2} + \mathcal{O}(a^4). \tag{2.47}$$

2.3 Numerical experiment

In this section, results from numerical experiments are presented. Everything is calculated in MatLab. First, to understand how a wave group consisting of two waves with different wave lengths can look, it is plotted a few examples in Figure 2.2. Just to simplify a bit, the waves all have the same amplitude, $a_1 = a_2 = 0.05$ m.

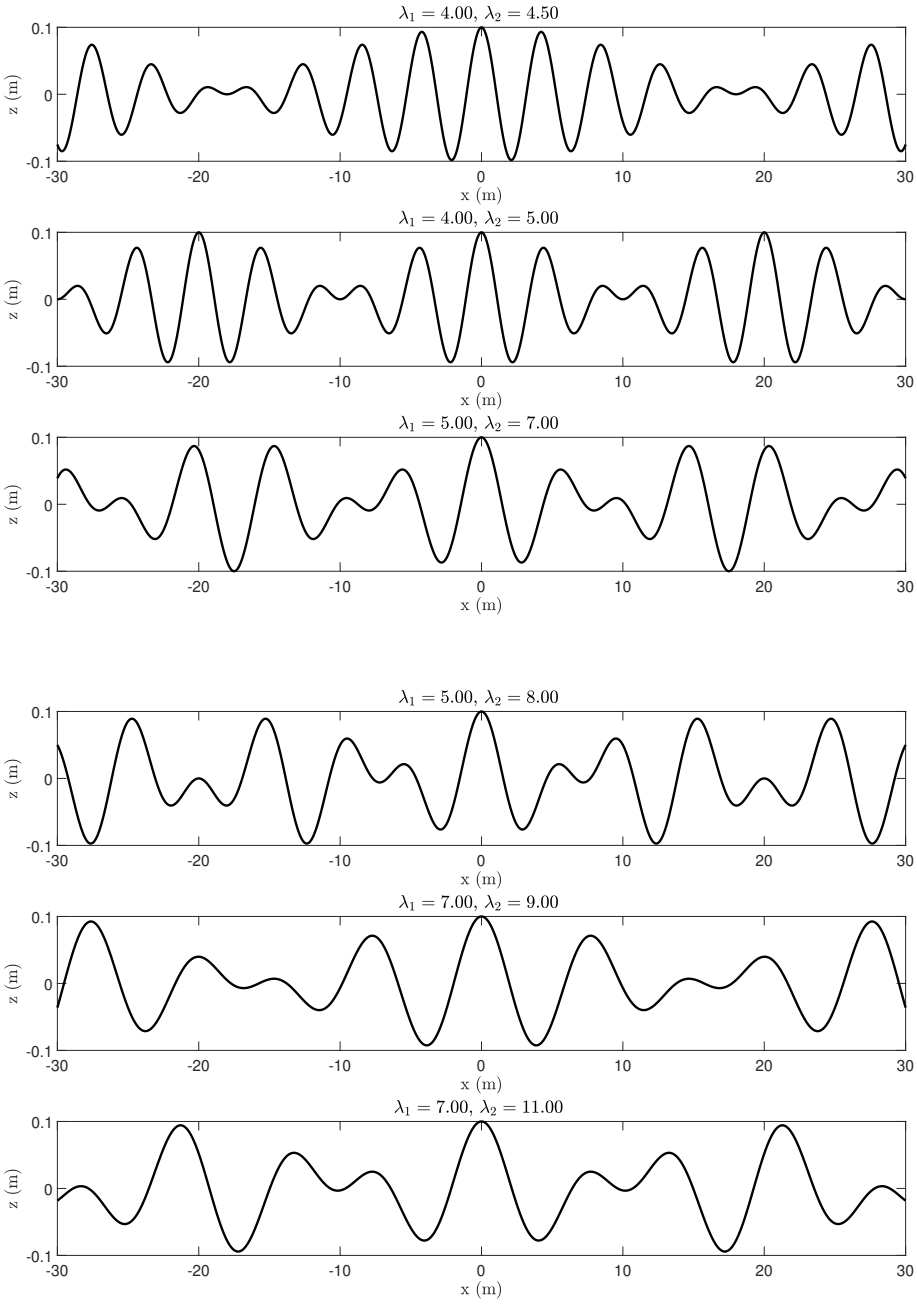

Figure 2.2: Wave groups with different wave lengths at depth $h = 100$ m .

If $a = a_1 = a_2$, the wave group is defined

$$\eta(x,t) = a\,\cos(k_1 x - \omega_1 t) + a\,\cos(k_2 x - \omega_2 t) \tag{2.48}$$

$$= 2a\,\cos(\frac{1}{2}\Delta k x - \frac{1}{2}\Delta\omega t)\cos(kx - \omega t) \tag{2.49}$$

and as before $\Delta k = k_1 - k_2$, $k = (k_1 + k_2/)2$, $\Delta\omega = \omega_1 - \omega_2$ and $\omega = (\omega_1 + \omega 2)/2$. It consists of one slowly varying wave and one progressive wave. The slow propagating wave $2a\,\cos(\frac{1}{2}\Delta k x - \frac{1}{2}\Delta\omega t)$ defines the envelope of the wave group. This wave has a long period: $T_{env} = 2\pi/(2\Delta\omega) = 4\pi/\Delta\omega$. The carrier wave has a shorter period: $T_{car} = 2\pi/\omega$ [11]. These two periods are calculated for the six different wave groups from Figure 2.2. In addition do we calculate the Stokes drift (with second order effects included) at the free surface. The results are presented in Table 2.1 and 2.2, evaluated at shallow and deep water respectively.

λ_1	λ_2	T_{car}	T_{env}	$\bar{u}_S\|_{z=\eta}$
4 m	4.5 m	1.73 s	45.12 s	0.0156 m/s
4 m	5 m	1.79 s	24.07 s	0.0135 m/s
5 m	7 m	2.07 s	17.26 s	0.0025 m/s
5 m	8 m	2.17 s	12.70 s	0.0005 m/s
7 m	9 m	2.76 s	26.35 s	-0.0105 m/s
7 m	11 m	2.96 s	15.54 s	-0.0145 m/s

Table 2.1: Period T_{car}, T_{env} and Stokes drift $\bar{u}_S$ for different wave groups at depth $h = 1$ m.

λ_1	λ_2	T_{car}	T_{env}	$\bar{u}_S\|_{z=\eta}$
4 m	4.5 m	1.65 s	55.97 s	0.0282 m/s
4 m	5 m	1.69 s	30.32 s	0.0264 m/s
5 m	7 m	1.93 s	23.11 s	0.0176 m/s
5 m	8 m	1.99 s	17.09 s	0.0164 m/s
7 m	9 m	2.25 s	36.86 s	0.0112 m/s
7 m	11 m	2.34 s	20.94 s	0.0100 m/s

Table 2.2: Period T_{car}, T_{env} and Stokes drift $\bar{u}_S$ for different wave groups at depth $h = 100$ m.

The Stokes drift is clearly larger for the waves in deeper water compared to the shallow water waves. The reason is due to the last term, $-Kc_g\frac{a_1^2+a_2^2}{gh-c_g^2}$, when calculating the Stokes drift. Since we divide by the depth h this term will decrease as the depth increase. In shallow water the second order effect is greater and cause the particles to drift slower. For wave lengths $\lambda_{1,2} = 7$, 9 and $\lambda_{1,2} = 7$, 11 the particles at the free surface are even drifting backwards even though the wave is propagating forward.

To understand more how the particles travel, particle trajectories also under the free surface are plotted. All four plots have end-time $t = 2 * T_{env}$, meaning the end-times are different for each wave. The particle trajectories in shallow water are plotted in Figure 2.3. These are found by using a ODE45-solver in MatLab.

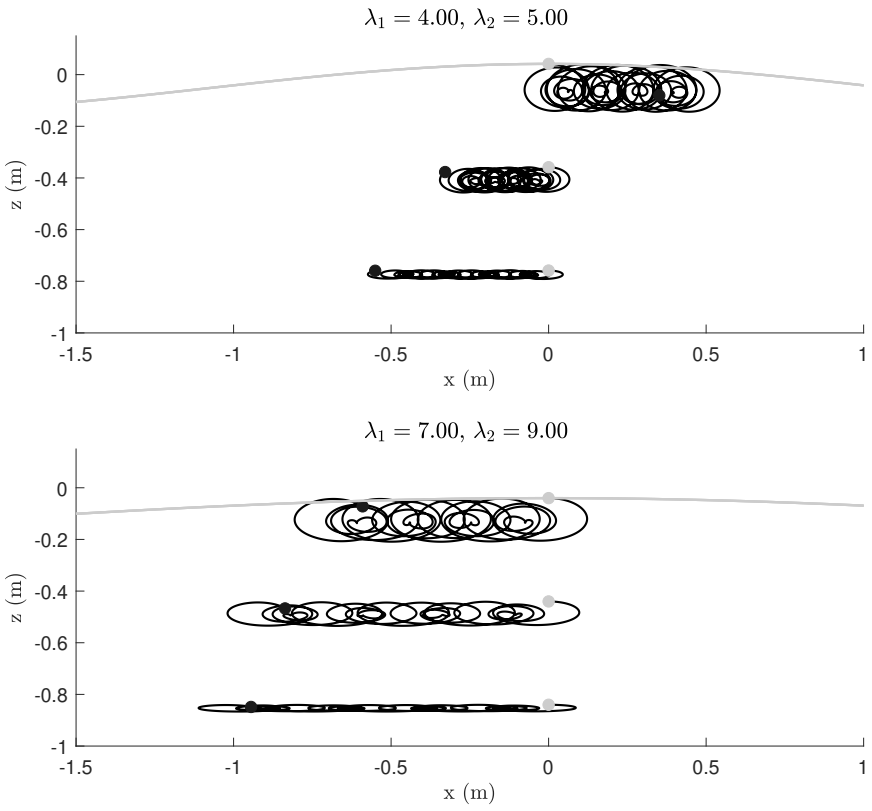

Figure 2.3: Shallow water ($h = 1$ m) particle trajectories at $z = \eta$, -0.4, -0.8 m. The light gray dot show the initial position and the black dot the end.

For the wave-group with $\lambda_{1,2} = 4$, 5, the particles at the free surface have a positive Stokes drift and are propagating in the same direction as the wave. Below the surface, the particles starts traveling in the opposite direction. Closer to the bottom, the negative Stokes drift is even larger.

Then the depth is changed to $h = 100$ m, but keeping the wave-lengths unchanged:

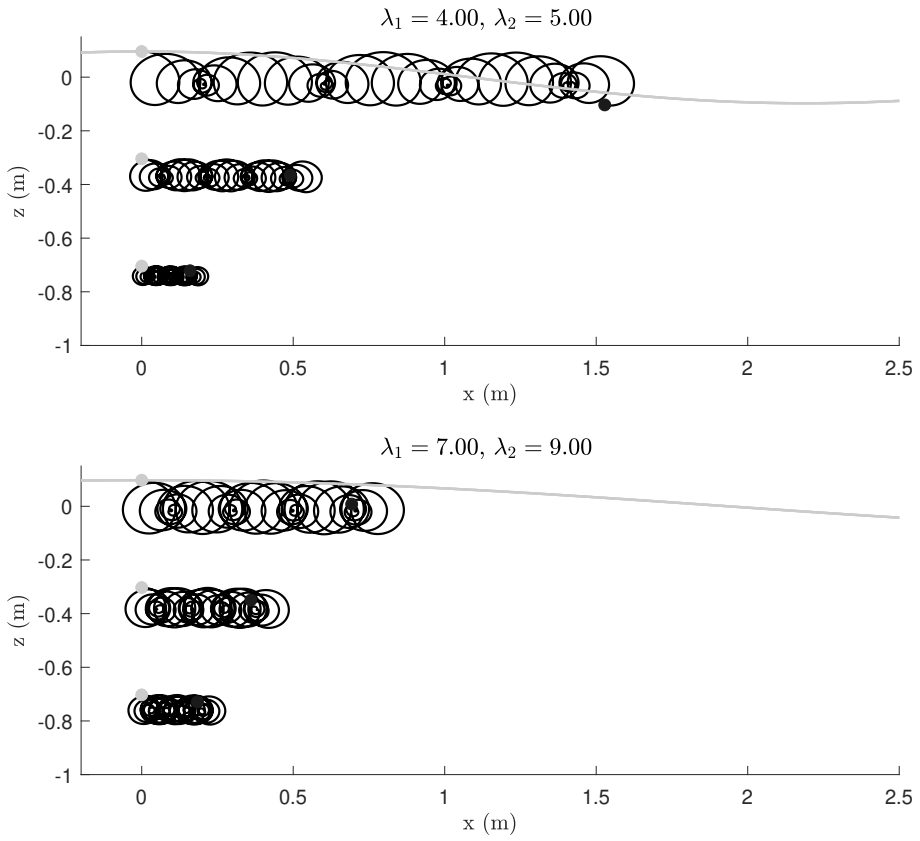

Figure 2.4: Deep water ($h = 100$ m) particle trajectories at $z = \eta$, -0.4, -0.8 m. The light gray dot show the initial position and the black dot the end.

All the particle trajectories show that the particles are drifting in the same direction as the wave. The Stokes drift is strongest at the free surface and decays with depth. It seems like the infra-gravity wave is insignificant regarding the mass-transport and Stokes drift in deep water. To understand this better

the Stokes drift $\bar{u}_S$ as a function of depth z is plotted in Figure 2.5. The black lines show the Stokes drift when the second theory is used. The red lines are the Stokes drift using only first order theory.

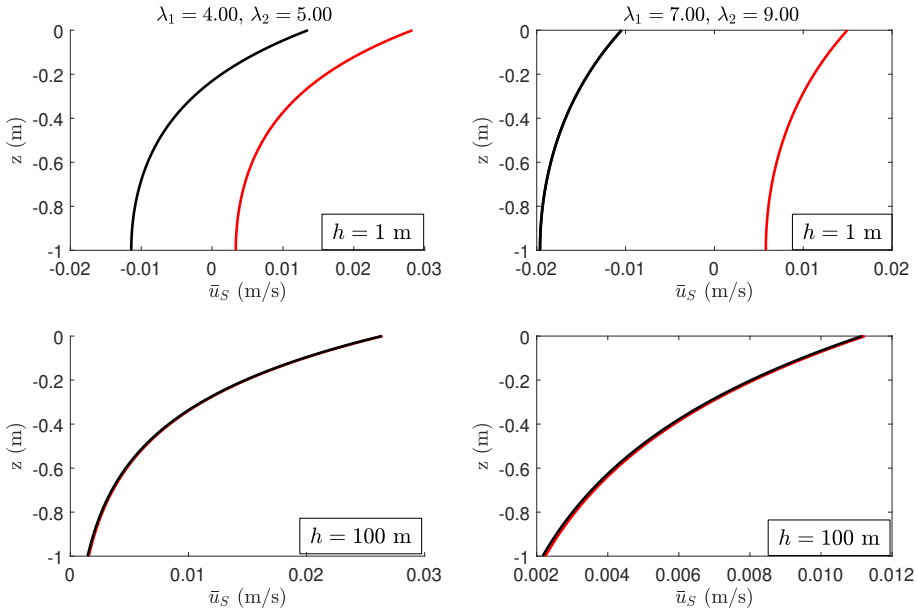

Figure 2.5: The Stokes drift as a function of depth z for the four waves in Figure 2.3 and 2.4. The black lines show the Stokes drift for the second order theory, which is the theory being used in this chapter. For comparison is also the first order theory Stokes drift plotted in red.

As seen in the two upper plots, which is for shallow water, there is a remarkable difference between using first or second order theory. For the two lower plots the difference between including the second order or not are of no consequence. This emphasizes the point made earlier, that the depth h decides how influential the infra-gravity wave will be. A last remark is that the velocity potential is not uniquely defined. It is possible to add a arbitrary function of x, meaning we can't know the true mass-transport just by doing numerical experiments.

Chapter 3

Non-linear theory

The linear theory which we defined in Chapter 1 is a good approximation in many cases. However, in shallow water this theory does not include dispersive effects. That means the waveform stays unchanged while propagation. We are therefore deriving the KdV-equation to model weakly non-linear dispersive waves [11].

3.1 The KdV-equation

The derivation of the KdV-equation is following Chapter 13 of [23].
In Chapter 1, we defined the free surface problem. The Laplace equation

$$\phi_{xx} + \phi_{ZZ} = 0 \tag{3.1}$$

has to be solved where Z now are the vertical distance from the bottom and $\phi_Z = 0$ at $Z = 0$. The velocity potential is written like

$$\phi = \sum_{n=0}^{\infty} Z^n \, f_n(x,t). \tag{3.2}$$

We then substitute (3.2) into (3.1):

$$\frac{\partial^2}{\partial x^2} \sum_{n=0}^{\infty} Z^n f_n(x,t) + \frac{\partial^2}{\partial Z^2} \sum_{n=0}^{\infty} Z^n f_n(x,t) = \tag{3.3}$$

$$\sum_{n=0}^{\infty} Z^n \frac{\partial^2 f_n(x,t)}{\partial x^2} + \sum_{n=2}^{\infty} n(n-1) Z^{n-2} f_n(x,t) = 0 \tag{3.4}$$

This is re-written by factoring out Z^n and changing the lower limit for the summation:

$$\sum_{n=0}^{\infty} Z^n \Big[\frac{\partial^2 f_n(x,t)}{\partial x^2} + (n+2)(n+1) f_{n+2}(x,t) \Big] = 0 \tag{3.5}$$

$$\implies f_{n+2} = \frac{-1}{(n+2)(n+1)} \frac{\partial^2 f_n}{\partial x^2}. \tag{3.6}$$

The solution to this recursion function is

$$f_{2n} = \frac{-1}{2n(2n-1)} \frac{\partial^2 f_{2n-2}}{\partial x^2} \tag{3.7}$$

$$= \frac{-1}{2n(2n-1)} \frac{\partial^2}{\partial x^2} \Big(\frac{-1}{(2n-2)(2n-3)} \frac{\partial^2 f_{2n-4}}{\partial x^2} \Big) \tag{3.8}$$

$$= \frac{1}{2n(2n-1)(2n-2)(2n-3)} \frac{\partial^4 f_{2n-4}}{\partial x^4} = ... = \frac{(-1)^n}{(2n)!} \frac{\partial^{2n} f_0}{\partial x^{2n}} \tag{3.9}$$

where only even terms are kept because $f_1 = 0$ due to the boundary conditions. Then, (3.2) is written as

$$\phi = \sum_{n=0}^{\infty} (-1)^n \frac{Z^{2n}}{(2n)!} \frac{\partial^{2n} f}{\partial x^{2n}} \tag{3.10}$$

where $f = f_0$. The next step is to substitute this expression into the boundary conditions. Before it is done, the variables are normalized:

$$x' = lx, \quad Z' = h_0 Z, \quad t' = \frac{lt}{c_0}, \quad \eta' = a\eta, \quad \phi' = \frac{gla\phi}{c_0} \tag{3.11}$$

where the original variables are primed. To make the analysis easier, the terms will be ordered by the dimensionless parameters $\alpha = a/h_0$ and $\beta = h_0^2/l^2$. Using the normalized variables, the Laplace equation is defined as:

$$\nabla^2 \phi = \frac{gla}{c_0 l^2} \frac{\partial \phi}{\partial x^2} + \frac{gla}{c_0 h_0^2} \frac{\partial^2 \phi}{\partial Z^2} = 0$$

$$\implies \beta \frac{\partial^2 \phi}{\partial x^2} + \frac{\partial^2 \phi}{\partial Z^2} = 0 \tag{3.12}$$

The same thing is done with the boundary conditions (1.12):

$$\begin{aligned} \phi_Z = 0, \quad & Z = 0 \\ \eta_t + \alpha \phi_x \eta_x - \frac{1}{\beta} \phi_Z = 0, \quad & Y = 1 + \alpha\eta \\ \eta + \phi_t + \frac{1}{2} \alpha \phi_x^2 + \frac{1}{2} \frac{\alpha}{\beta} \phi_Z^2 = 0, \quad & Y = 1 + \alpha\eta \end{aligned} \tag{3.13}$$

The last thing to normalize is the expansion of ϕ which then looks like

$$\phi = \sum_{n=0}^{\infty} (-1)^n \frac{Z^{2n}}{(2n)!} \frac{\partial^{2n} f}{\partial x^{2n}} \beta^n. \tag{3.14}$$

This is substituted into the kinematic boundary condition:

$$\eta_t + \alpha \frac{\partial}{\partial x} \Big(\sum_{n=0}^{\infty} (-1)^n \frac{Z^{2n}}{(2n)!} \frac{\partial^{2n} f}{\partial x^{2n}} \beta^n \Big) \eta_x - \frac{1}{\beta} \frac{\partial}{\partial Z} \Big(\sum_{n=0}^{\infty} (-1)^n \frac{Z^{2n}}{(2n)!} \frac{\partial^{2n} f}{\partial x^{2n}} \beta^n \Big) \tag{3.15}$$

$$= \eta_t + \alpha \Big(\sum_{n=0}^{\infty} (-1)^n \frac{Z^{2n}}{(2n)!} \frac{\partial^{2n+1} f}{\partial x^{2n+1}} \beta^n \Big) \eta_x - \frac{1}{\beta} \Big(\sum_{n=1}^{\infty} (-1)^n \frac{Z^{2n-1}}{(2n-1)!} \frac{\partial^{2n} f}{\partial x^{2n}} \beta^n \Big) = 0 \tag{3.16}$$

The terms are then ordered by powers of β. Since it is a surface boundary condition is $Z = 1 + \alpha\eta$. That leads to

$$\eta_t + \big((1+\alpha\eta) f_x \big)_x - \big[\frac{1}{6} (1+\alpha\eta)^3 f_{xxxx} + \frac{1}{2} \alpha (1+\alpha\eta)^2 f_{xxx} \eta_x \big] \beta + \mathcal{O}(\beta^2) = 0 \tag{3.17}$$

For the dynamic boundary condition, the same approach is used and

$$\eta + f_t + \frac{1}{2} \alpha f_x^2 - \frac{1}{2} (1+\alpha\eta)^2 \Big[f_{xxt} + \alpha f_x f_{xxx} - \alpha f_{xx}^2 \Big] \beta + \mathcal{O}(\beta^2) = 0. \tag{3.18}$$

Next all terms of $\mathcal{O}(\beta)$ for (3.17) and (3.18) are kept, but terms of $\mathcal{O}(\alpha\beta)$ are being dropped. The dynamic boundary condition is also differentiated with respect to x. This gives the normalized Boussinesq-equations which looks like

$$\begin{aligned} &\eta_t + \big[(1+\alpha\eta) w \big]_x + \mathcal{O}(\alpha\beta, \beta^2) = 0 \\ &w_t + \alpha w w_x + \eta_x - \frac{1}{2} \beta w_{xxt} + \mathcal{O}(\alpha\beta, \beta^2) = 0 \end{aligned} \tag{3.19}$$

where $w = f_x$ is the first term in the expansion of the velocity in the horizontal direction:

$$u = \phi_x = w - \beta \frac{Z^2}{2} w_x x + \mathcal{O}(\beta^2). \tag{3.20}$$

By just keeping the lowest orders of (3.19) we yield

$$\eta_t + w_x + \mathcal{O}(\alpha, \beta) = 0 \tag{3.21}$$

$$w_t + \eta_x + \mathcal{O}(\alpha, \beta) = 0. \tag{3.22}$$

The KdV-equation is a uni-directional wave, so we are only interested in the right going solution which looks like:

$$w = \eta, \quad \eta_t + \eta_x = 0. \tag{3.23}$$

Hence, a solution of (3.19) up to first order in α and β in the form

$$w = \eta + \alpha A + \beta B + \mathcal{O}(\alpha^2 + \beta^2) \tag{3.24}$$

is looked for. A and B are functions of η and its x-derivatives. Inserting this into (3.19) gives

$$\eta_t + \eta_x + \alpha\big[A_x + 2\eta\eta_x\big] + \beta\big[B_x - \frac{1}{6}\eta_{xxx}\big] + \mathcal{O}(\alpha^2 + \beta^2) = 0 \tag{3.25}$$

$$\eta_t + \eta_x + \alpha\big[A_t + \eta\eta_x\big] + \beta\big[B_t - \frac{1}{2}\eta_{xxt}\big] + \mathcal{O}(\alpha^2 + \beta^2) = 0 \tag{3.26}$$

The two equations are consistent if $A = -\frac{1}{4}\eta^2$ and $B = \frac{1}{3}\eta_{xx}$. Inserting this into the upper of the equations gives the normalized Korteweg-deVries equation

$$\eta_t + \eta_x + \frac{3}{2}\alpha\eta\eta_x + \frac{1}{6}\beta\eta_{xxx} + \mathcal{O}(\alpha^2 + \beta^2) = 0 \tag{3.27}$$

which in the dimensional form is expressed as

$$\eta_t + c_0\eta_x + \frac{3}{2}\frac{c_0}{h_0}\eta\eta_x + \frac{1}{6}h_0^2\eta_{xxx} = 0. \tag{3.28}$$

By setting $h_0 = 1$ and $g = 1$, we have the

$$\eta_t + \eta_x + \frac{3}{2}\eta\eta_x + \frac{1}{6}\eta_{xxx} = 0 \tag{3.29}$$

where h_0 is a unit of distance and $\sqrt{h_0/g}$ as a unit of time [5].

3.2 Periodic solution of the KdV

The KdV-equation can be solved exactly for both solitary and periodic waves. The solitary wave is the easiest equation to obtain from the KdV-equation, but we are going to solve for the periodic solution called the cnoidal wave. This wave is known for sharper crests and flatter troughs than the sinusoidal-wave. The derivation of the cnoidal wave uses [5], [8] and[14] as a reference. Assuming the cnoidal wave is of constant shape, we make the guess

$$\eta(x,t) = f(\xi) \quad , \qquad \xi = x - ct. \tag{3.30}$$

This can be substituted into the KdV-equation (3.29) and we obtain an ordinary differential equation

$$-cf' + f' + \frac{3}{2}ff' + \frac{1}{6}f''' = 0. \tag{3.31}$$

Integrating once yields

$$(1-c)f + \frac{3}{4}f^2 + \frac{1}{6}f'' = \frac{1}{4}A \tag{3.32}$$

where A is an integration constant. We then multiply by f' and integrate again

$$\frac{1}{3}(f')^2 = -f^3 + 2(c-1)f^2 + Af + B = F(f) \tag{3.33}$$

where B is an integration constant which has to be positive for the solution to be periodic. Since this is a third order polynomial, it can be written

$$F(f) = -(f - f_1)(f - f_2)(f - f_3) \tag{3.34}$$

where f_1, f_2 and f_3 are the roots. By comparing (3.33) and (3.34) we have these relations:

$$\begin{aligned} f_1 + f_2 + f_3 &= 2(c-1) \\ f_1f_2 + f_2f_3 + f_3f_1 &= -A \\ f_1f_2f_3 &= B > 0 \end{aligned} \tag{3.35}$$

The last expression gives three options for f_1, f_2 and f_3:

- All three roots are positive
- One root is positive, while two roots are complex conjugate
- One root is positive and two are negative

The first option is not possible because it would mean $\eta > 0$ and therefore lie above the mean water level for all values. The second option would result in unbounded values for η. We are then left with the third option.

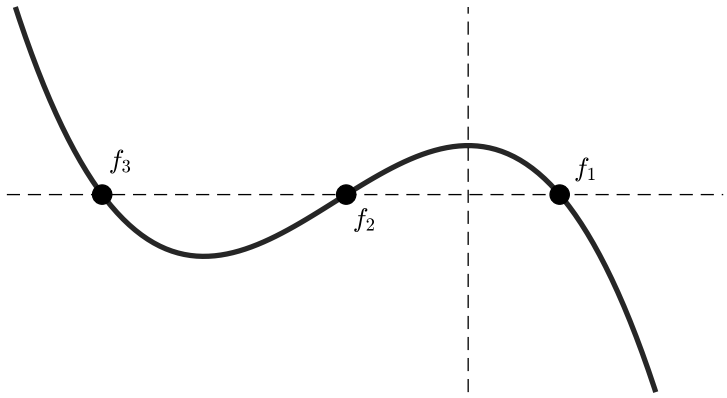

Figure 3.1: The function $F(f)$ with two negative roots and one positive.

It is necessary that

$$f_2 \leq f \leq f_1 \tag{3.36}$$

for the derivative f' to be real and bounded. We can then conclude that f_1 is the crest's amplitude and f_2 of the trough. A solution for f which is periodic and inside this range is given as

$$f(\xi) = f_1 \cos^2 \chi(\xi) + f_2 \sin^2 \chi(\xi) \tag{3.37}$$

This expression is then substituted into the left hand side of (3.33):

$$\frac{1}{3}\Big(\frac{\partial f}{\partial \xi}\Big)^2 = \frac{4}{3}\Big(\frac{\partial \chi}{\partial \xi}\Big)^2 \cos^2 \chi(\xi) \sin^2 \chi(\xi) (f_1 - f_2)^2 \tag{3.38}$$

and into (3.34). By some re-writing we yield

$$F(f) = (f_1 - f_2)^2 \cos^2 \chi(\xi) \sin^2 \chi(\xi)[(f_1 - f_3) - (f_1 - f_2) \sin^2 \chi(\xi)]. \tag{3.39}$$

Putting the equations together, we obtain

$$\frac{4}{3}\Big(\frac{\partial \chi}{\partial \xi}\Big)^2 = (f_1 - f_3) - (f_1 - f_2) \sin^2 \chi(\xi). \tag{3.40}$$

This is re-written as

$$\sigma^2\Big(\frac{\partial \chi}{\partial \xi}\Big)^2 = 1 - m \sin^2 \chi(\xi) \tag{3.41}$$

where the abbreviations are defined as

$$\sigma^2 = \frac{4}{3(f_1 - f_3)} \quad , \qquad m = \frac{f_1 - f_2}{f_1 - f_3}. \tag{3.42}$$

We know that $f_3 < f_2 < f_1$, which means $0 < m < 1$. Then (3.41) is integrated and we get

$$\frac{1}{\sigma}\int_{\xi_0}^{\xi} d\tilde{\xi} = \pm \int_{\chi(\xi_0)=0}^{\chi} \frac{d\tilde{\chi}}{\sqrt{1 - m\sin^2\tilde{\chi}}}. \tag{3.43}$$

The right hand side is called the incomplete elliptic integral of the first kind, where m is called the elliptic parameter. If we call the integral $\mathrm{F}(\chi|m)$, we have

$$\frac{\xi - \xi_0}{\sigma} = \mathrm{F}(\chi|m). \tag{3.44}$$

The phase ξ is given as a function of χ. The inverse functions are called the cosine-elliptic and sine-elliptic functions and are defined as

$$\begin{aligned} \cos\chi &= \mathrm{cn}(\frac{\xi - \xi_0}{\sigma}|m) \\ \sin\chi &= \mathrm{sn}(\frac{\xi - \xi_0}{\sigma}|m). \end{aligned} \tag{3.45}$$

The elliptic integrals are called complete when $\chi = \pi/2$. The complete integrals of first and second kind are defined

$$K(m) = \int_0^{\pi/2} \frac{d\tilde{\chi}}{\sqrt{1 - m\sin^2\tilde{\chi}}} \quad , \quad E(m) = \int_0^{\pi/2} \sqrt{1 - m\sin^2\tilde{\chi}}\, d\tilde{\chi}. \tag{3.46}$$

Finally, substituting (3.45) back into (3.37) and changing the variables back yields

$$\eta(x,t) = f_2 + (f_1 - f_2)\mathrm{cn}^2\Big(\frac{\sqrt{3(f_1 - f_3)}}{2}(x - ct - x_0)\Big|m\Big) \tag{3.47}$$

where the fact that $\mathrm{cn}^2 + \mathrm{sn}^2 = 1$ is used. We then obtained what is called the cnoidal wave, which is the periodic solution of the KdV-equation. Hence, we see that f_2 has to be the lowest point and f_1 the highest since $0 < \mathrm{cn}^2 < 1$. The wave height is then simply defined as $H = f_1 - f_2$. We also want to find an expression for the wave length λ and phase speed c.

If we look at (3.37), when $\chi(\xi_1) = 0, 2\pi, ..$ we obtain the crest and the trough at $\chi = \pi/2, 3\pi/2, ...$ The distance from crest to trough is $\pi/2$ in terms of $\chi(\xi_2)$, which means λ would be twice of this. Using (3.43) we find the wave length to be

$$\lambda = 2\int_{\xi_1}^{\xi_2} d\tilde{\xi} = 2\sigma \int_0^{\pi/2} \frac{d\tilde{\chi}}{\sqrt{1 - m\sin^2\tilde{\chi}}} = 2\sigma K(m). \tag{3.48}$$

The phase speed c is found by comparing (3.33) and (3.34):

$$\begin{aligned} 2(c-1)f^2 &= (f_1+f_2+f_3)f^2 \\ \implies c &= 1+\frac{1}{2}(f_1+f_2+f_3) \end{aligned} \tag{3.49}$$

Finally, it is seen that the cnoidal wave is fully defined by the three parameters f_1, f_2 and f_3. However, the wave can also be defined by the wave height H, elliptic parameter m and mean-water level $\bar{\eta}_0$.

We start with

$$\int_0^\lambda \eta(x,t)dx = 2\int_{\xi_1}^{\xi_2} f_2 + (f_1-f_2)\mathrm{cn}^2\Big(\frac{\xi}{\sigma}|m\Big)d\xi = \bar{\eta}_0\lambda \tag{3.50}$$

By changing the variables from ξ to χ using (3.37) and (3.41) we obtain

$$\begin{aligned} \bar{\eta}_0\lambda &= 2\int_{\chi(\xi_1)=0}^{\chi(\xi_2)=\pi/2} (f_1\cos^2\chi + f_2\sin^2\chi)\frac{d\xi}{d\chi}d\chi \\ &= 2\sigma\int_0^{\pi/2} \frac{f_1(1-\sin^2\chi)+f_2\sin^2\chi}{\sqrt{1-m\sin^2\chi}}d\chi \\ &= 2\sigma\int_0^{\pi/2} \frac{f_1-(f_1-f_2)\sin^2\chi}{\sqrt{1-m\sin^2\chi}}d\chi \\ &= 2\sigma\int_0^{\pi/2} \frac{f_1-m(f_1-f_3)\sin^2\chi}{\sqrt{1-m\sin^2\chi}}d\chi \\ &= 2\sigma\int_0^{\pi/2} (f_1-f_3)\sqrt{1-m\sin^2\chi} + \frac{f_3}{\sqrt{1-m\sin^2\chi}}d\chi \\ &= 2\sigma\Big((f_1-f_3)E(m)+f_3K(m)\Big) \end{aligned}$$

We are then left with

$$\bar{\eta}_0 = (f_1-f_3)E(m)+f_3K(m) \tag{3.51}$$

which in addition to $H = f_1 - f_2$ and $m = (f_1-f_2)/(f_1-f_3)$ enables us to define the parameters f_1, f_2 and f_3 by H, m and $\bar{\eta}_0$:

$$\begin{aligned} f_1 &= \frac{H}{m}\Big(1-\frac{E(m)}{K(m)}\Big)+\bar{\eta}_0 \\ f_2 &= \frac{H}{m}\Big(1-m-\frac{E(m)}{K(m)}\Big)+\bar{\eta}_0 \\ f_3 &= -\frac{H}{m}\frac{E(m)}{K(m)}+\bar{\eta}_0 \end{aligned} \tag{3.52}$$

The wave is now defined if the wave height H, elliptic parameter m and mean-water level $\bar{\eta}_0$ is known.

Chapter 4

Comparing mass-transport for linear and non-linear shoaling waves

This chapter is using a code written by H. Kalisch and H. Borluk [3] to calculate the particle paths for the cnoidal wave. The code was later modified and improved by Olufemi E. Ige.

4.1 Introduction

As waves approach a sloping beach, the waves are getting shorter and steeper until they eventually break. Decreasing depth h also leads to a change in the mean water level $\bar{\eta}_0$. Before the break point a set-down occurs, meaning a negative mean water level. As there is no energy loss, the radiation stress increases. Theory presented by Longuet-Higgings and Stewart [13] gives the magnitude of this set-down. It is defined as

$$\bar{\eta}_0 = -\frac{1}{8} H_0^2 k_0 \frac{\coth^2(kh)}{2kh + \sinh\, 2kh}. \tag{4.1}$$

In 1968, Bowen *et al.* [4] did an experiment where they compared measurements of the mean water level to (4.1). They find the theory to match the results well, before the wave becomes too steep and breaks due to the sloping beach. Non-linear waves approaching a beach are more complicated as the velocity depends

on the wave height in lowest order of approximation. A method for the change of wave height as the cnoidal wave is getting closer to the shore was done by Svendsen and Brink-Kjær in 1973 [18]. The Svendsen and Brink-Kjær's article was some of the groundwork for Khorsand and Kalisch as they continued working on the change of wave height for a shoaling solitary wave [10]. There has also been experiments on the particle paths regarding the cnoidal wave. Chen *et al.* [7]) did an experiment where particles were traced and compared to fifth-order theory. This was however calculated for a uniform depth. The velocity field and particle paths for the KdV-equation were in 2012 derived by Borluk and Kalisch [3], that we are using in this article. Recently a study on the shoaling waves using the KdV-equation was done by Paulsen [17].

This article will combine the shoaling and particle paths of linear and non-linear waves. The wave height and wave number are found at different depths. Then the particle paths are calculated. The Stokes drift of both linear and non-linear waves are calculated for comparison. The waves are all evaluated before they break down. The wave height, period and mean water level will be experimental data from Bowen *et al.* [4].

The experiment was done in a wave tank that was 40 meters long, 0.75 meter deep and 0.5 meter wide. A wave with known height, frequency and wave length is approaching a smooth beach with slope 4.7° ($\tan\ \beta = 0.082$). As seen in Figure 4.1, the wave then experiences a small set-down before the set-up and breaking. The mean water level $\bar{\eta}_0$ was found by using manometer to calculate the static pressure. The theory corresponds well with the actual mean water level up until the wave is getting close to breaking. Then theory and measurement start to diverge.

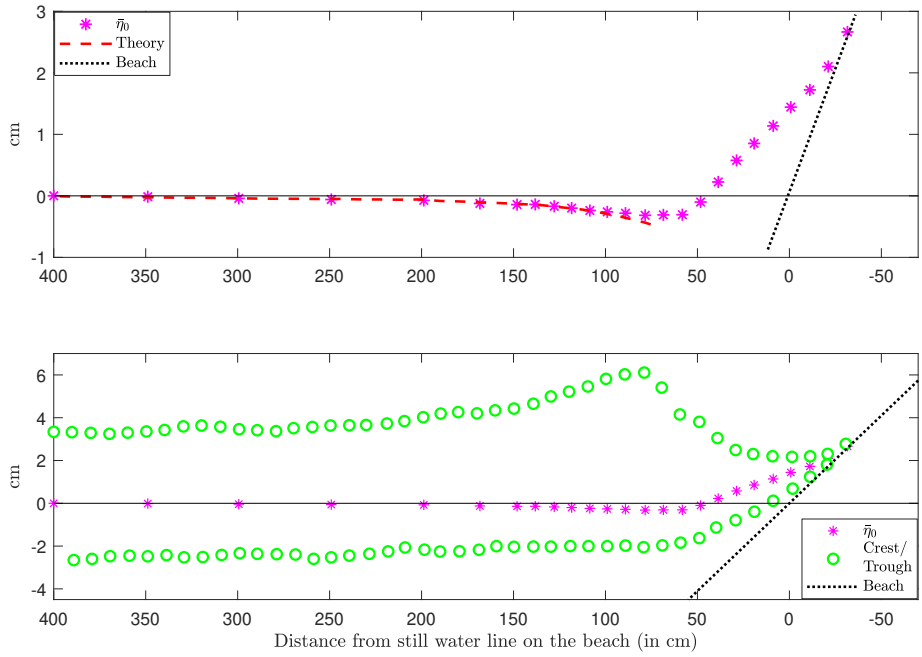

Figure 4.1: Upper: The measured mean water level $\bar{\eta}_0$ compared to the theoretical. Lower: The measured $\bar{\eta}_0$, crest and trough for the same wave as above.

We want to know about the wave and the associated mass-transport when the theory is still valid. Since the linear theory explains the set-down, a sinusoidal-wave is first found.

4.2 Linear theory

The linear wave looks like

$$\eta = a\,\cos(kx - \omega t) + \bar{\eta}_0 \tag{4.2}$$

where $\bar{\eta}_0$ is the mean water level. The goal is to find a wave that matches the data from the experiment.
At $x = 110$ cm $= 1.10$ m the experimental and theoretical $\bar{\eta}_0$ are still the same. The depth at this position is found to be $h = 0.090$ m. The period of the wave is given as $T = 1.14$ s. The frequency $\omega = 2\pi/1.14$ s is assumed to be constant [10], even though the wave is approaching the beach. Using MatLab,

the wave-number k is found using the dispersion relation:

$$\omega^2 - \sqrt{kh\ \tanh(kh)} = 0. \tag{4.3}$$

The wave height before the shoaling is $H_0 = 0.0645$ m. The wave height H at a given depth is

$$H = H_0 \sqrt{\frac{C_{g,0}}{C_g}} \tag{4.4}$$

where $C_{g,0}$ is the velocity before the wave approaches the beach. The local velocity at the given depth is C_g [10]. By using the formula to find $\bar{\eta}_0$ (4.1), we have all the variables needed to define a linear wave:

$$\eta = 0.0335\ \cos(6.1043x - 5.4722t) - 0.0027. \tag{4.5}$$

4.2.1 Mass-transport for the linear wave

To find the mass-transport, it is necessary to figure out how the mean water level $\bar{\eta}_0$ affects the velocity field. It could be thought of as an infinitely long wave:

$$\lim_{k\to 0} \bar{\eta}_0\, cos(kx - \omega t) = \bar{\eta}_0\, cos(0) = \bar{\eta}_0. \tag{4.6}$$

The horizontal and vertical velocity are then defined as

$$\begin{aligned} \lim_{k\to 0} u &= \lim_{k\to 0} \bar{\eta}_0 \sqrt{gk\ \tanh(kh)} \frac{\cosh(k(z+h))}{\sinh(kh)} \cos(kx - \omega t) \\ &= \bar{\eta}_0 \sqrt{gk\, kh} \frac{1}{kh} \cos(0) \\ &= \bar{\eta}_0 \sqrt{\frac{g}{h}} \end{aligned} \tag{4.7}$$

$$\begin{aligned} \lim_{k\to 0} w &= \lim_{k\to 0} \bar{\eta}_0 \sqrt{gk\ \tanh(kh)} \frac{\sinh(k(z+h))}{\sinh(kh)} \sin(kx - \omega t) \\ &= \bar{\eta}_0 \sqrt{gk\, kh} \frac{k(z+h)}{kh} \sin(0) \\ &= 0. \end{aligned} \tag{4.8}$$

The mean-water level changes the horizontal velocity only. We can see that the effect of a set-up or a set-down will be larger for small depths. For deep water, we see that $\bar{\eta}_0 \sqrt{g/h} \approx 0$.

The wave is plotted in Figure 4.2. In addition did we plot the same wave, but without any set down. Then their respective particle trajectories are plotted.

Even though the difference in mean water level seems small, it impacts the particle paths. After $t = 5T$, the surface particles from the wave with no set down have clearly drifted furthest.

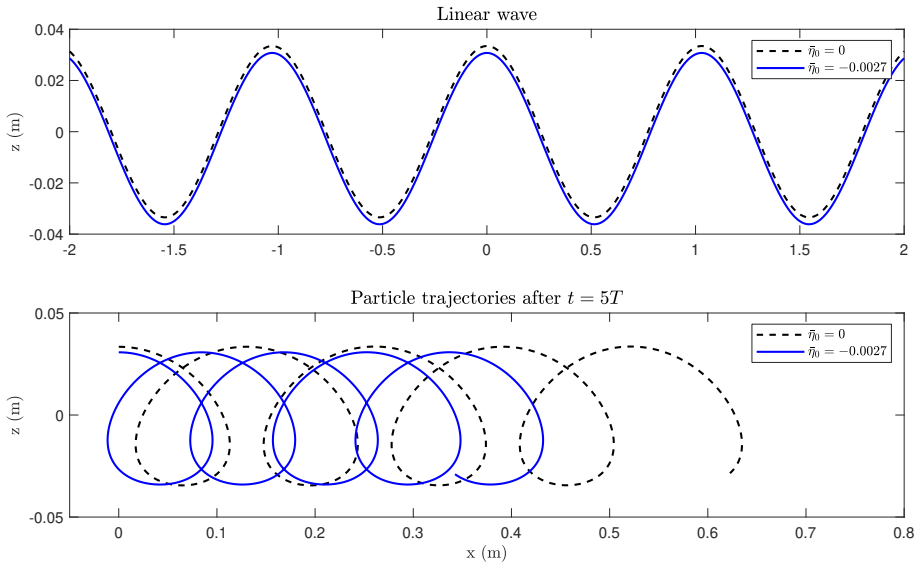

Figure 4.2: Upper: Linear waves with the same period $T = 1.14$ s, but different $\bar{\eta}_0$. Lower: The surface particle paths for the waves above.

Then the Stokes drift $\bar{u}_S$ for the two waves is calculated. It is defined as

$$\bar{u}_S = a^2 \omega k \frac{\cosh(2k(z_0 + h))}{2\sinh^2(kh)} + \bar{\eta}_0 \sqrt{\frac{g}{h}}. \tag{4.9}$$

The wave with a set down has Stokes drift $\bar{u}_S = 0.0628$ m/s at the surface. The other wave is drifting at a velocity of $\bar{u}_S = 0.0934$ m/s. This means that in this case a set down of only -0.0027 m reduces the velocity by $\approx 30\%$. With a larger set-down, the particles could drift backwards even though the wave is propagating forward.

4.3 Non-linear theory

The linear theory could explains the mean water level well. We also found the amplitude and mass-transport by using linear theory. However, by looking at Figure 4.1 we see that the wave can't be linear. If the wave was a cosine-wave and had a set-down, the magnitude of the crest would have to be less than the trough. Here it is opposite, meaning the wave has a different shape. The cnoidal wave is a non-linear wave with sharp crests and flat troughs. It is possible for the wave to have a set-down even though the crest is larger than the trough, meaning it could fit to our problem. This wave is found by an exact solution of the KdV-equation.

The KdV-equation is an equation describing waves at the surface where the fluid is inviscid and incompressible. The equation is derived under some certain conditions. The waves are assumed to have a small amplitude a and long wave-length λ compared to the undisturbed depth h. To be more precise it means that the parameters $\alpha = a/h$ and $\beta = h^2/\lambda^2$ should be of the same order, along with being small. This is the Boussinesq regime. Additionally the motion of the wave has to be in one direction. The equation is non-dimensional where h is a unit of distance and $\sqrt{h/g}$ a unit of time. It then looks like:

$$\eta_t + \eta_x + \frac{3}{2}\eta\eta_x + \frac{1}{6}\eta_{xxx} = 0. \tag{4.10}$$

The periodic wave solution to (4.10) gives the cnoidal wave. It is defined by three parameters f_1, f_2 and f_3. The surface is given as

$$\eta(x,t) = f_2 + (f_1 - f_2)\mathrm{cn}^2\Big(\frac{\sqrt{3(f_1 - f_3)}}{2}(x - ct - x_0)\Big) \tag{4.11}$$

where the wave height is defined as $H = f_1 - f_2$. This means that f_1 is the crest and f_2 is the trough. The wave speed is $c = 1 + \frac{1}{2}(f_1 + f_2 + f_3)$ and $m = \frac{f_1 - f_2}{f_1 - f_3}$ is the elliptic parameter. The wave length is defined as $\lambda = 2\sigma K(m)$ where $\sigma^2 = \frac{4}{3(f_1 - f_3)}$ [5].

It is also possible to define the three parameters f_1, f_2 and f_3 by the wave height

H, the elliptic parameter m and the equilibrium level $\bar{\eta}_0$ [17]:

$$\begin{aligned} f_1 =& \frac{H}{m}\big(1 - \frac{E(m)}{K(m)}\big) + \bar{\eta}_0 \\ f_2 =& \frac{H}{m}\big(1 - m - \frac{E(m)}{K(m)}\big) + \bar{\eta}_0 \\ f_3 =& -\frac{H}{m}\frac{E(m)}{K(m)} + \bar{\eta}_0. \end{aligned} \tag{4.12}$$

The goal is to find a cnoidal wave that is equivalent to the experiment regarding the period, depth and set-down.
We see from Figure 4.1, that f_1 and f_2 are already given. The wave height at $x = 1.10$ m from shore and depth $h = 0.09$ m is then

$$H = f_1 - f_2 = 0.0546 - (-0.0200)\text{ m} = 0.0746\text{ m}. \tag{4.13}$$

We then need to find the elliptic parameter m. If we choose m so that the period gets correct, $T = 1.14$ s, there is not enough freedom to choose $\bar{\eta}_0$. We prioritize to get the right period and find $m = 0.99937$. This gives $\bar{\eta}_0 = -0.0053$, which does not match up with the experimental set-down. The reason is that the wave height is too big compared to the depth, which violates the Boussinesq regime. We are still calculating the mass-transport using this theory, even though a higher-order non-linear theory would be more correct to use.

In the linear case, the set down only shifts the wave down. As seen in Figure 4.3, this is not the case for the non-linear theory. The two waves have the same period and wave height, but because of the non-linearity different wave lengths and phase speeds.

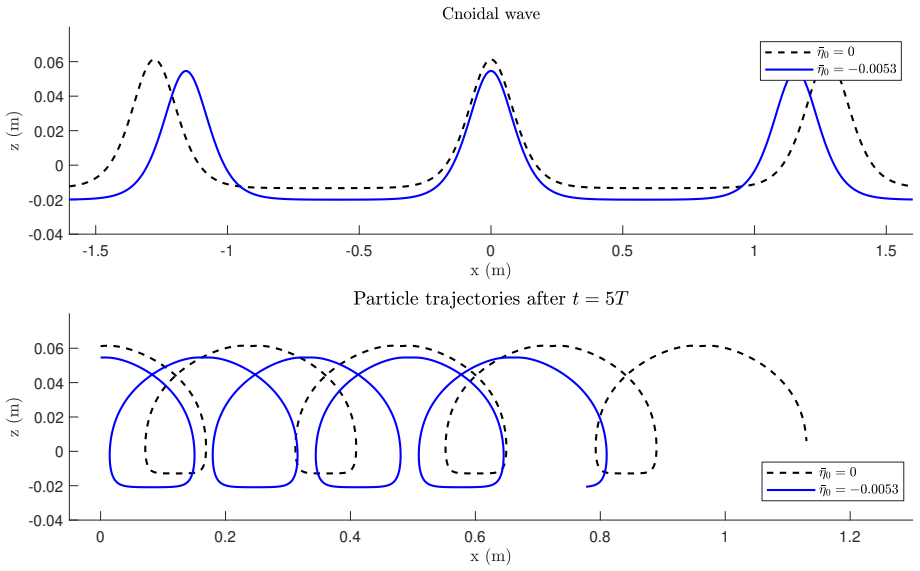

Figure 4.3: Upper: Cnoidal wave with the same period $T = 1.14$ s, but different $\bar{\eta}_0$. Lower: The particle paths at the surface for the waves.

4.3.1 Mass-transport for the cnoidal wave

To find the Stokes drift of the two cnoidal waves the Lagrangian period T_L needs to be found. This is calculated by finding the time where the particle reaches the same z-value as the initial one. When the Lagrangian period is found, it is possible to find the x-value at this time. Then the Stokes drift will be $\bar{u}_s = \Delta x / T_L$.

For the wave with no set down, the particles are drifting $\bar{u}_s = 0.1887$ m/s. For the other wave, which has $\bar{\eta}_0 = -0.0053$ m, the Stokes drift is $\bar{u}_s = 0.1345$ m/s. The set down is slowing the wave down by around $\approx 30\%$.

4.4 Discussion

We now used both linear and non-linear theory to reconstruct the experimental wave from Bowen, Simmons and Inman [4] at one specific depth. The result is summarized in Table 4.1. The two waves have the same period, $T = 1.14$ s.

	H (m)	$\bar{\eta}_0$ (m)	$\bar{u}_S$ (m/s)
Linear wave	0.0670	-0.0027	0.0628
	0.0670	0	0.0934
Non-linear wave	0.0746	-0.0053	0.1345
	0.0746	0	0.1887

Table 4.1: Wave height H, mean water level $\bar{\eta}_0$ and Stokes drift $\bar{u}_S$ for the wave at $h = 0.090$ m.

From the table, we see that the linear and non-linear wave give two different results. The wave height for the linear wave is found theoretically by equation (4.4). The non-linear wave's wave height is from the experimental data, using the crest and trough. This means that the linear wave height estimate is too low at this depth. Regarding the mean water level $\bar{\eta}_0$, the linear theory works well as seen in Figure 4.1. The non-linear theory evaluates the set-down to be approximately twice of the experimental. The Stokes drift $\bar{u}_S$ using non-linear theory gives a mass-transport that's double compared to the linear theory. What causes this difference, is hard to tell. On the one hand the cnoidal wave has a larger amplitude, which could mean a larger mass-transport. On the other hand, it has a larger set-down which slows the mass-transport down. The shape of the two waves are different, which affects the way the particles move.
Up until now we only looked at the wave right before it starts to break. At this depth the linear and non-linear theory are not in agreement.

To understand more of the wave shoaling, we find the wave heights and Stokes drift at different depths. In Figure 4.4, the experimental wave height H is compared with linear theory at different depths.

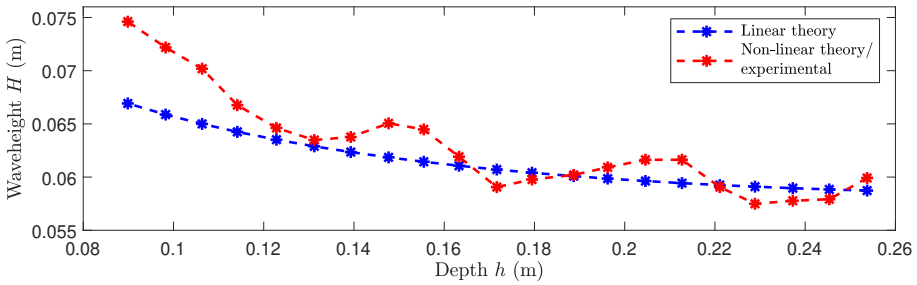

Figure 4.4: Comparison of the non-linear wave height H found from the crest and trough (Figure 4.1) and the theoretical wave height using linear theory, equation (4.4).

We see that the non-linear and experimental wave height are the same. This is because we use the measured crest and trough when we define the cnoidal wave. The random variations in wave height might be due to measuring errors. Still, we see that with decreasing depth the wave heights are increasing overall. Using linear theory results in a steadily increasing wave height. For 0.12 m $< h <$ 0.26 m, the wave heights don't differ too much between the two theories. For $h <$ 0.12 m, we see that the experimental wave height grows more rapidly compared to the linear theory approximations. The wave gets steeper right before it breaks and linear theory is no longer valid.

In Figure 4.5, we find the Stokes drift for linear and non-linear waves at different depths. It is found using the same procedure as in Section 4.2.1 and 4.3.1.

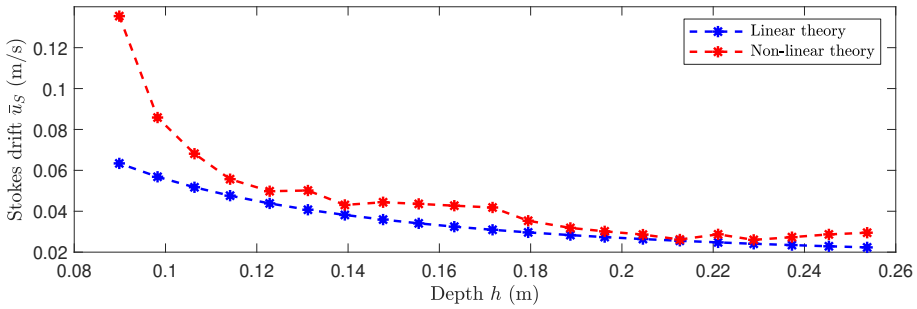

Figure 4.5: Stokes drift at different depths using both linear and non-linear theory.

The result resembles the comparison of wave heights in Figure 4.4. The non-linear theory gives a slightly larger mass-transport for all depths, but the two curves follow each other up until $h \approx 0.11$ m. As the wave travels even closer to the beach, the difference between linear and non-linear theory gets bigger. If we look at how the wave changes with depth, this makes sense. In Figure 4.6, the wave from the experiment is plotted at three different depths.

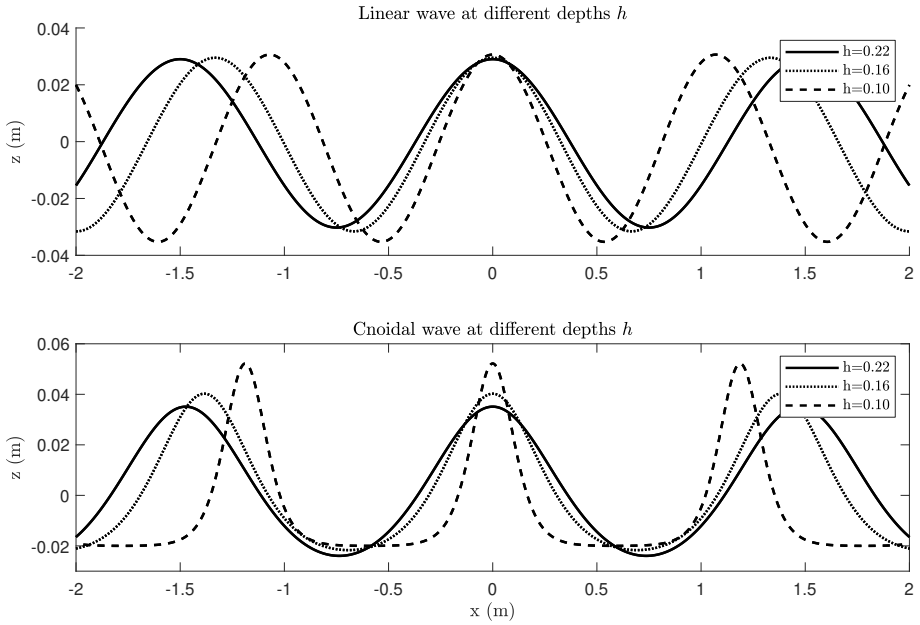

Figure 4.6: The wave profile of the linear and cnoidal wave for three different depths. The upper plot uses linear theory and the lower non-linear.

From the figure, we observe that the shape of the linear and cnoidal wave are quite similar for $h = 0.22$ m and $h = 0.16$ m. The cnoidal wave is a bit steeper with a somewhat larger mass-transport. At $h = 0.10$ m, the cnoidal wave has sharper crests and flatter troughs. The shape do no longer look like a sinusoidal-wave.

To summarize, the linear theory explains the mean water level for shoaling waves up until the wave starts to break well. However, the linear theory is not sufficient to explain the wave's amplitude and mass-transport close to the break zone. The waves are too steep and simply not linear. The non-linear theory

used in this article could explain the mass-transport to some degree. Thus, the water gets too shallow for this theory to be completely correct. Further from shore, the linear theory is enough to find the mass-transport. We did also see that a small change in the mean water level impacts the mass-transport.

Chapter 5

Field experiment

In this chapter, a field experiment done in September 2019 will be presented. The project was done in collaboration with the Institute of Coastal Research in Helmholtz-Zentrum Geesthacht, which supplied all the equipment. Before we get into the details, an overview and context of the experiment will be given.

The location for the experiment was Sylt in Germany, which is an island close to the border of Denmark. We were three people from University of Bergen and six from Helmholtz-Zentrum Geestacht, which is a German research institute. The project was mainly planned by Henrik Kalisch (University of Bergen) and Marc Buckley (Helmholtz-Zentrum Geestacht). The goal was to understand more about what impacts the mass-transport by doing both Lagrangian and Eulerian measurements. To do the Lagrangian measurements, you would need some sort of particle tracer. The idea of berries first came to mind, but it was quickly figured out they would be too small and hard to track. The decision landed on using oranges instead. Even though the orange has inertia, it is floating at the free surface. In addition, the round shape is convenient and the bright color makes it easier to see. The measurements were done at a beach on the western coast of the island. Doing field experiments are really unpredictable and strong wind was a huge challenge for these measurements. However, the last day gave us good weather just in time and was enough to collect the data needed.

Figure 5.1: Upper: Group photo of the people from the field study. Lower: The beach were the experiments took place.

The results from the field experiment are to be found in the submitted paper "Lagrangian Measurements of Orbital Velocities in the Surf Zone" [2]. In this chapter my contributions to the paper are explained. The work of transforming the raw data into usable data sets was done by Maria Bjørnestad and Michael Streßer. But, firstly the experimental set-up will be explained in more details.

5.1 Experimental set-up and data analysis

The set-up of the experiment is shown in Figure 5.2. Six poles were installed into the sand. The distance between the poles varied from 8.4 to 12.6 meters. Pole 1 was approximately 80 meters from the shoreline and furthest away. At every pole, there was also placed a pressure gauge (PG). This makes it possible to measure the surface elevation. Close to pole 2, an acoustic Doppler velocimeter (ADV) was put in place to measure the Eulerian flow. Two pairs of cameras, CMOS digital cameras with Canon 50 mm and 400 mm lenses, were placed on a hill watching over the surf zone. The distance between the cameras was about 40 meters. The field of view for the two cameras is overlapping and shown in the figure. The oranges, being the particle tracers, were deployed between pole 1 and 2 by a swimmer.

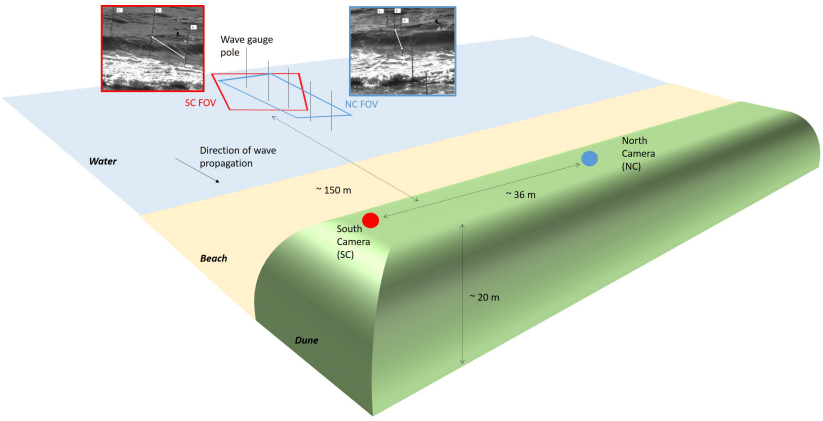

Figure 5.2: Set-up of the experiment. The poles are numbered with 1 being the furthest from the beach and 6 the closest. The particle tracers were deployed between pole 1 and 2. The coordinate-system sets sea bottom at pole 2 to be the origin. This figure was made by Marc Buckley.

As the oranges were deployed into the sea, the cameras took pictures at 30 frames/second. Through data analysis done by Maria Bjørnestad, the positions of the oranges were projected onto the xz-plane. The coordinate-system has origin at bottom of pole 2. The x-axis is then showing the distance from pole 2, with positive direction being shoreward. The z-axis shows the distance from the sea bottom to the free surface.

In the upper part of Figure 5.3, the surface elevation of four waves is plotted. It is constructed from the pressure gauge installed at pole 2. To get the waves centred around zero, the mean over a 10 minute period is subtracted. The waves are then zero-crossed upwards. For each wave the average is found and represented by the black lines. The lower part of Figure 5.3 shows the Lagrangian motion of one orange riding on three waves. The three paths correspond to the three waves in the same color in the upper part of the figure.

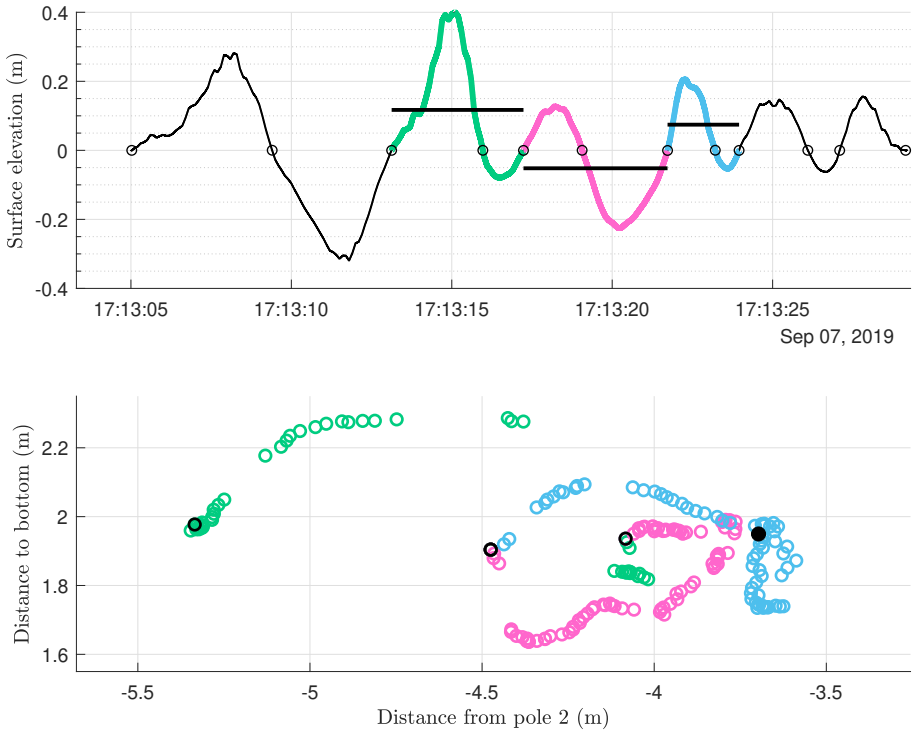

Figure 5.3: Upper: The time-series of the surface elevation at pole 2. It was constructed from the pressure gauge measurements. The time series is zero-crossed upwards and the black lines show the mean water level for each wave. Lower: The Lagrangian motion of one orange. The particle path of the orange is color coded, where the wave in the upper plot correspond to the path in the same color. The black circles show where the path starts. The black dot show where the path stops for the blue wave. The data analysis was done by Michael Streßer and Maria Bjørnestad.

The oranges were located close to the middle between pole 1 and 2. The distance between the two poles is 11.11 meters. From GPS-positions it is known that the depth at pole 1 is 0.36 meters greater than at pole 2. The depth in between is not known exactly, but if the beach was a straight line, the slope would be 1.85°. In addition to the x and z-positions, the timestamp for each position was also given.

Before analyzing the oranges, the z-axis is adjusted. This was done individually for every wave by adding $\Delta h = \frac{0.36}{11.11}|\bar{x}|$ to the z-positions of the oranges, where $\bar{x}$ is the mean of the horizontal orange position for each wave.

The goal of the next section is to investigate how well a theoretical wave matches the particle tracer of the experiment. The methods of finding these theoretical particle paths are described in the following section. Both linear and non-linear theory are used.

5.2 Methods for finding particle tracer path

5.2.1 Linear theory

The linear wave is defined like

$$\eta(x,t) = \frac{H}{2} cos(kx - \omega t) + (h + \bar{\eta}_0) \tag{5.1}$$

where η now is the distance from the sea bottom to the free surface. When the wave is defined, the particle path at a given position can be found.

The first thing to be done, is finding the maximum z_{max} and minimum z_{min} of the orange path. From those values the wave height H and average depth $\bar{z}$ are defined:

$$H = z_{max} - z_{min} \tag{5.2}$$

$$\bar{z} = \frac{z_{max} + z_{min}}{2} \tag{5.3}$$

The depth h and mean water level $\bar{\eta}_0$ are unknown. They are defined by the known value $\bar{z}$:

$$\bar{z} = h + \bar{\eta}_0. \tag{5.4}$$

This means that it is enough to find either h or $\bar{\eta}_0$. The last parameter to be found is the period T. From this the radian frequency ω is defined. The spatial frequency k can also be found if T is known, through the dispersion relation.

In MatLab T and $\bar{\eta}_0$ are found such that

$$\underset{T,\bar{\eta}_0}{min}||(\xi,\zeta)-(x,z)||_2, \tag{5.5}$$

where (ξ,ζ) are the positions of the theoretical particle path and (x,z) are the positions of the oranges for one given path.

The function minimizing the distance needs an initial point for the parameters to be fitted. For the period T, the fact that we have the timestamp for each orange is taken advantage of. As the orange goes for approximately one Lagrangian period, the end time of the path will give an estimate of that. The Lagrangian period is known to be a bit longer than the Eulerian, but it is still a valid initial guess. From zero-crossing analysis of the waves at pole 2, a mean water level is given. This will then be the initial point of $\bar{\eta}_0$.

5.2.2 Non-linear theory

For the non-linear theory, a similar procedure is used to find a cnoidal wave. The wave height H is defined in the same way as for the linear theory, by finding the maximum and minimum $z-$position. Since the KdV-equation is used in non-dimensional form, the wave heights are divided by the depth h: $H = f_1 - f_2 = \frac{z_{max}-z_{min}}{h}$. Like before, the depth h is not known and needs to be found. The last parameter needed to define a cnoidal wave is f_3 which is depending on the elliptic parameter m: $f_3 = f_1 - \frac{H}{m}$.
Then the problem is again solved in MatLab to find the particle path closest to the oranges:

$$\underset{h,m}{min}||(\xi,\zeta)-(x,z)||_2. \tag{5.6}$$

The code for calculating the theoretical particle path (ξ,ζ) was written by Borluk and Kalisch [3]. It was later modified and improved by Olufemi E. Ige. For the initial value of the depth, the average depth $\bar{z}$ is used. With the elliptic parameter m, the initial guess was adjusted for each wave depending on the shape of the orange path. When the depth h and elliptic parameter m were found, everything was scaled back to the original dimensions again.

5.3 Comparing linear and non-linear particle paths

In this section, the green, pink and blue paths from Figure 5.3 will be compared with both linear and non-linear waves. The grey dot indicates the starting point of the path. The black dot shows the end point. The measured positions of the particle tracer are plotted in orange. The black line is the theoretical particle path.

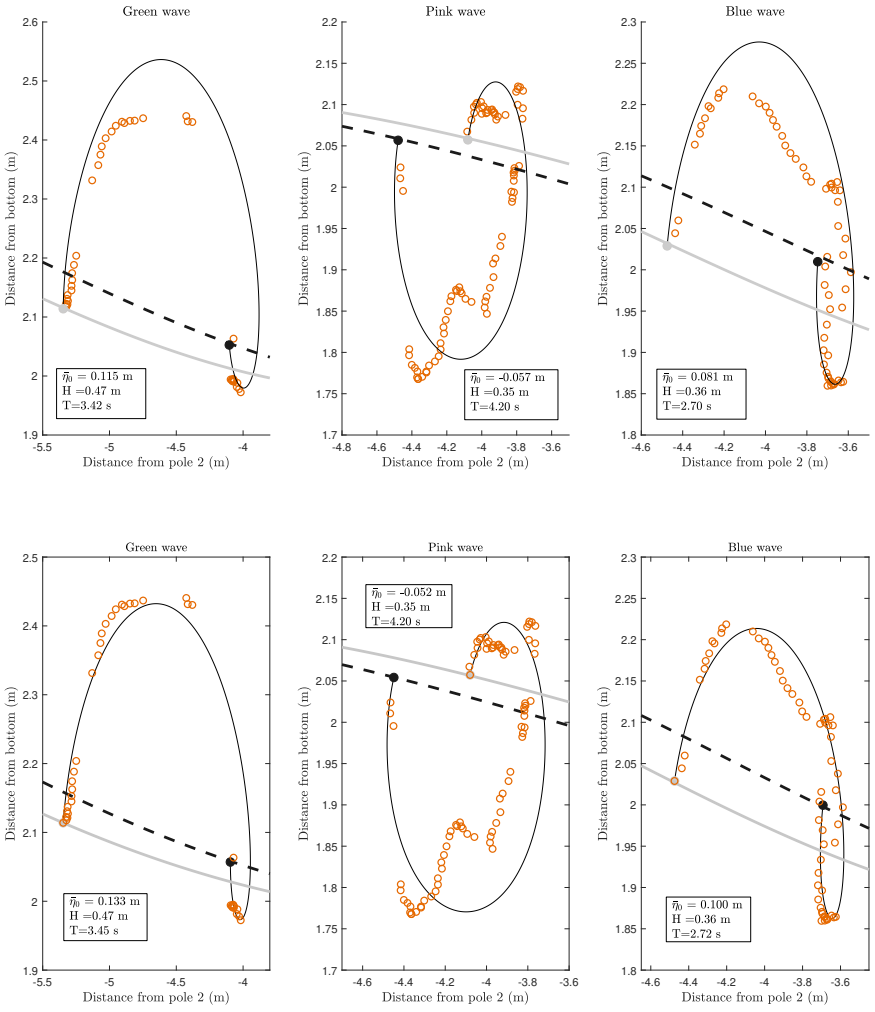

Figure 5.4: Particle paths calculated from linear theory (upper) and non-linear theory (lower). The orange circles are the measured positions of the particle tracer.

For each time step, the distance from the orange to the theoretical path is calculated. This difference is then plotted in Figure 5.5 below:

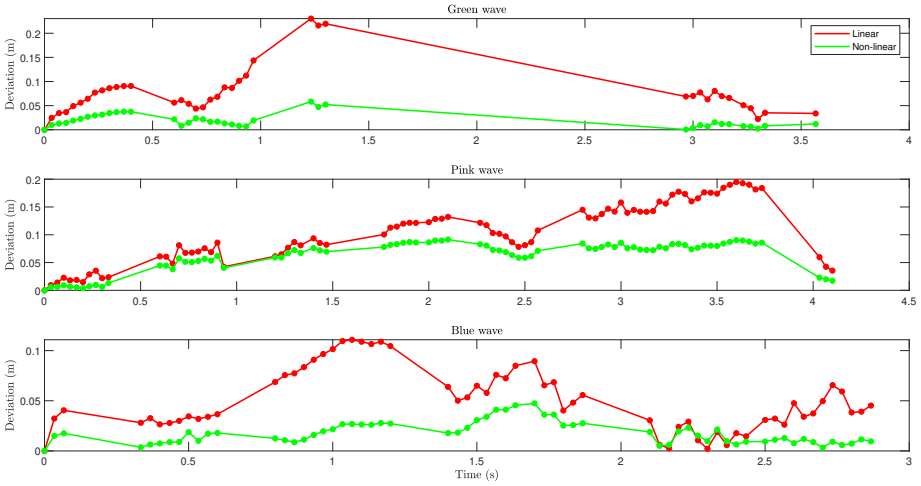

Figure 5.5: Comparison of the deviation between the observed and theoretical path, for linear and non-linear waves. The deviation is the distance between the orange and the estimated particle path for each time step.

The non-linear theory gives a smaller deviation for all three waves. For the green wave, the non-linear theory fits almost perfect. The error is small throughout the whole path. The elliptic parameter m decides the shape of the cnoidal wave. For $m \to 0^+$, it becomes a cosine-wave. The non-linear limit $m \to 1$, gives a solitary wave [5]. The cnoidal wave approximating the green particle path has $m = 0.62$. This means the wave will have sharper crests and wider troughs than the linear cosine wave. With a relatively high elliptic parameter, it makes sense that linear and non-linear theory give different results.

The particle path belonging to the pink wave is more messy than the two others. It goes slow at the top and has a bump in the middle of the path. This makes it hard to fit with both linear and non-linear theory.

Similar to the green wave the deviation is small when using non-linear theory to approximate the blue wave's particle path. The linear theory also gives a smaller deviation compared to the two waves above. This might be because the

elliptic parameter is $m = 0.30$ and closer to the linear limit $m = 0$.

For the linear and cnoidal waves found above, we know the wave lengths and mean water level $\bar{\eta}_0$. These numbers will be compared in Table 5.1 with values from the actual data. To find the wave length, this formula is used: $\lambda = cT$. The phase speed c for each wave is found by measuring the time the wave takes from pole 1 to pole 2. Since the distance between the poles is known, an estimate of the phase speed can be found. The period T is not known, but set to be the time of one full orange path. That is an over-estimate meaning the actual wave length might be a bit shorter. At the other hand, the phase speed is also an estimate so it is impossible to get an exact answer. The observed $\bar{\eta}_0$ is the average value for each wave from the surface elevation at pole 2.

		Measured	Linear theory	Non-linear theory
Green wave	λ	17.996 m	13.623 m	15.327 m
	$\bar{\eta}_0$	0.117 m	0.115 m	0.133 m
Pink wave	λ	17.604 m	17.189 m	16.076 m
	$\bar{\eta}_0$	-0.052 m	-0.057 m	-0.052 m
Blue wave	λ	13.908 m	9.708 m	10.677 m
	$\bar{\eta}_0$	0.074 m	0.081 m	0.100 m

Table 5.1: Comparing wavelengths and mean water level

The measured wave lengths are longer compared to the wave lengths calculated from theory. This makes sense because the period used is probably too high. It is reasonable that the wave lengths differ by a few meters as the method contains a lot of uncertainty.

The values for the mean water level are quite consistent for all three waves. A variation of a few centimeters can be explained by many reasons. The pressure measurements and the oranges are a few meters apart. This means that the wave can change a bit from the oranges to where the mean water level is measured. We don't know the depth either, so the still water level for the surface elevation might be wrong by a few centimeters.

5.4 Total mass-transport

Until now only the free surface particle paths have been studied. To understand more of the total mass-transport, we calculate the particle paths further down in the water column as well. Since the non-linear theory was better to approximate the orange paths, this is the theory being proceeded. In Figure 5.6, theoretical particle paths are plotted further down in the water column.

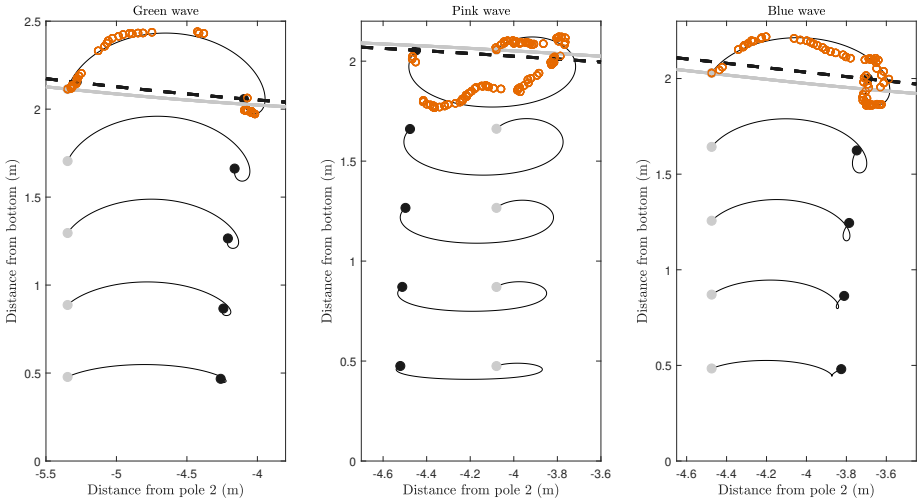

Figure 5.6: Particle paths calculated from non-linear theory at different depths in the water column.

From the figure it is seen that the green and blue wave experience a large forward drift throughout the water column. In contrast, the pink wave's particles are drifting backwards. This is connected to the mean-water level $\bar{\eta}_0$. A positive $\bar{\eta}_0$ makes the particle drift faster forward. For a negative $\bar{\eta}_0$ it is opposite. Calculating the correlation r between the mean water level and average flow halfway trough the water column measured by the ADV, gave $r \approx 0.70$ [2]. Thus, the mean water level has a great impact on the total mass-transport

5.5 Fourier analysis

This section uses Chapter 5.8 of [19] as a reference.
The three waves analyzed above were parts of a 10 minute time-series of the surface elevation. This is plotted in Figure 5.7.

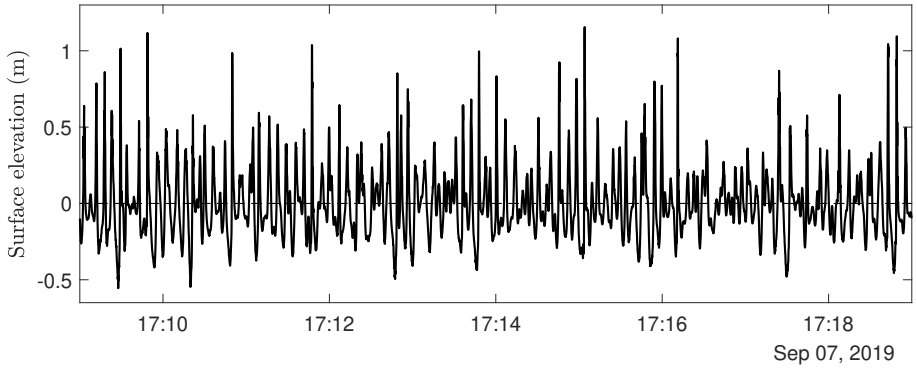

Figure 5.7: Ten minute time-series of the surface elevation.

We want to see if there are any lower-frequency waves in the record that cause the different mean water levels, like in Chapter 2. Here we also saw that the low-frequency wave was in phase with the wave group. By doing a Fourier Analysis, we can find the most influential frequencies for the time-series which is hard to find by just looking at it.

The sampling period for the pressure gauge was $\Delta t = 0.1$ s. This means that the highest detectable frequency, named the Nyquist frequency, is $f_N = 1/2\Delta t = 1/(2 \cdot 0.1 \text{ s}) = 5$ Hz. The lowest frequency, called the fundamental frequency, is found to be $f_0 = 1/N\Delta t = 1/(5999 \cdot 0.1 \text{ s}) = 0.0017$ Hz.
The discrete, finite Fourier series looks like

$$y(t_n) = \frac{1}{2}A_0 + \sum_{p=1}^{N/2} \left[A_p \; cos(2\pi pn/N) + B_p \; sin(2\pi pn/N)\right] \tag{5.7}$$

with the coefficients

$$A_p = \frac{2}{N} \sum_{n=1}^{N} y_n \; cos(2\pi pn/N), \tag{5.8}$$

$$B_p = \frac{2}{N} \sum_{n=1}^{N} y_n \; sin(2\pi pn/N), \tag{5.9}$$

$$p = 0,\, 1,\, 2\,, ..., N/2. \tag{5.10}$$

It is possible to write the Fourier series in a more compact form

$$y(t_n) = \frac{1}{2} C_0 + \sum_{p=1}^{N/2} C_p \cos\left[(2\pi pn/N) - \theta_p\right] \tag{5.11}$$

where

$$C_p = \left(A_p^2 + B_p^2\right)^{1/2}, \qquad \theta_p = \tan^{-1}[B_p/A_p]. \tag{5.12}$$

Accordingly, each frequency f has an amplitude C_p. This gives the importance of that specific frequency in the signal. The amplitudes are relative and can only be understood in context of each other. To find the dominant frequencies, a Fast Fourier Transform function in MatLab is applied. In Figure 5.8 the amplitude C_p for each frequency is plotted. The figure only includes $0 < f < 1$ Hz because the frequencies higher have $C_p \approx 0$ and are therefore not interesting.

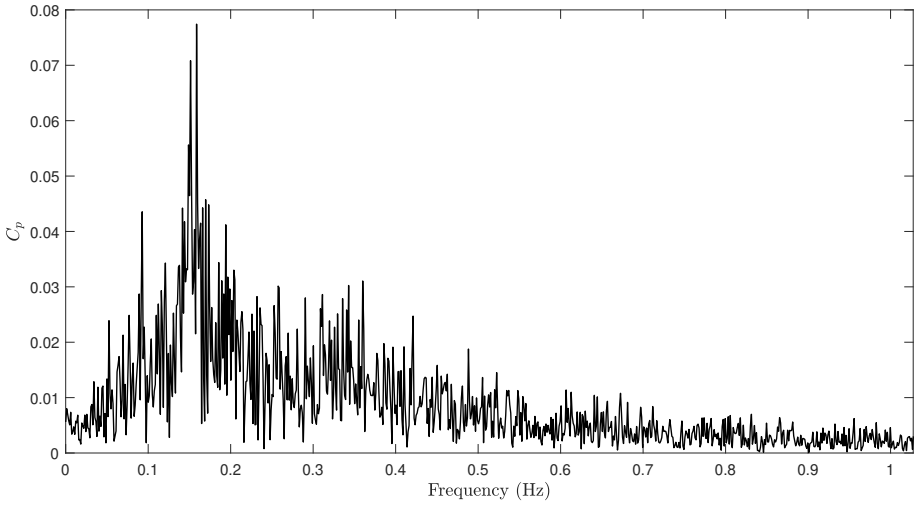

Figure 5.8: The amplitude C_p for each frequency between 0 and 1 Hz.

From this figure, we see that most waves are in the range $0.1 < f < 0.4$ Hz, or in other words $2.5 < T < 10$ s. The highest amplitudes are centered around $f = 0.15$ Hz, which corresponds to $T = 6.67$ s. We want to filter out the high frequency signal in the time series by using a lowpass-filter in MatLab. The frequency response of the filter being used on the time-series is shown in Figure 5.9.

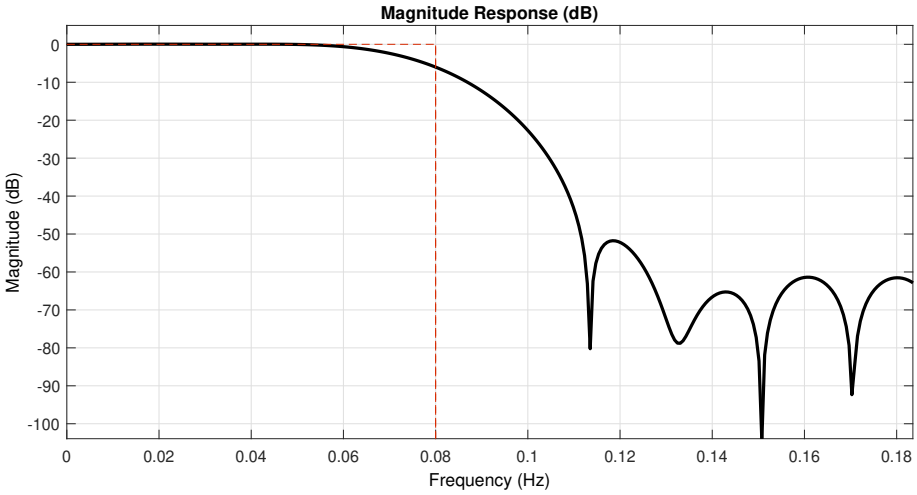

Figure 5.9: The filter being used on the time-series. The cut-off frequency was set to $f = 0.08$ Hz.

This shows how the filter attenuate the high-frequencies. The dB-scale is defined as

$$\text{dB} = 20 \log_{10} \frac{C_{\text{filt}}}{C_p}. \tag{5.13}$$

where C_{filt} is the amplitude of a frequency f after the filtering and C_p is the amplitude found by the Fourier analysis. If the amplitude remains unchanged like we want for the low frequencies, $C_{\text{filt}} = C_p$ and $\text{dB} = 20 \log_{10} \frac{C_p}{C_p} = 0$. If $\text{dB} = -20$, the filter has attenuated the amplitude at that specific frequency by a factor of 10. The filter used here, keeps the frequencies up until about $f = 0.06$ Hz unchanged. At $f = 0.08$ Hz, $C_{\text{filt}} = 0.5 C_p$. The result of the filtering is showed in Figure 5.10. The red line shows the filtered time-series on the original data in black.

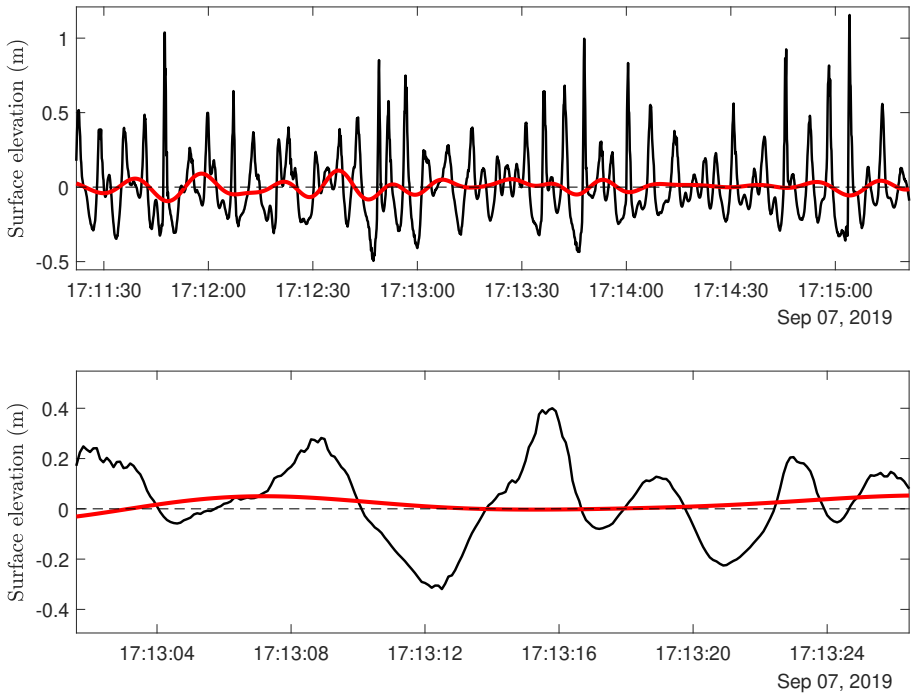

Figure 5.10: The time-series after a low-pass filter is applied. The lower plot is a zoomed-in version, which shows the waves analyzed earlier in this chapter.

From the filtering, an infra-gravity wave causing the differences in set-up and set-down is not seen. The low-frequency signal in red appears a bit random. In the lower picture we see the waves we have analyzed in this chapter. It is not possible to tell the mean-water level from this signal. Outgoing infra-gravity waves are created by the oscillations of the surf zone [6], meaning there could be low-frequency waves traveling in both directions. These might cancel or interact with each other, leaving us without a clear low-frequency signal.

To make sure the filtering works, we compare with the wave-groups from Chapter 2. We see that the filtering returns a clear low-frequency signal which is showed in Figure 5.11.

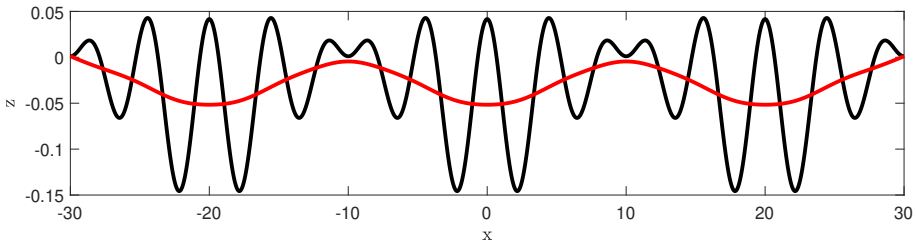

Figure 5.11: The filtered wave-group from Chapter 2 in red using a low-pass filter. The un-filtered data are plotted in black.

Chapter 6

Conclusion

To conclude this thesis, we summarize the main results. We first calculated the Stokes drift for different wave-groups. The wave-groups consisted of two waves added together with different wave lengths. The distance in wave length between the two waves was also differing. For shallow water the second order current was slowing the particles down compared to if it was not included. For some of the wave groups surface particles did even drift in the opposite direction to the wave propagation. When we compared the mass-transport using first and second-order in deep water, there was no difference.

For the shoaling waves it was seen that the linear theory predicted the set-down of the wave before breaking well. However, the shape of wave was clearly not linear. By using non-linear theory instead, we tried to fit a cnoidal wave to the given data. The crest, trough, period and mean-water level were given from the experiment. We were not able to model a cnoidal wave matching the mean water level to the experimental data while keeping the period and wave height correct. For future work, a higher order non-liner theory that also could match the mean-water level should be used to calculate the mass-transport.

The field-experiments were done in the surf zone meaning the waves are shoaling. The waves did not have a consistent set-down like before they were breaking, like we saw in Chapter 4. Neither did we see a bounded infra-gravity wave when we filtered the surface elevation time-series. There could be low-frequency

waves traveling in both directions caused by the oscillating surf-zone canceling each other. Nevertheless, it was clear that the mass-transport increased with increasing mean-water level and opposite. This is in agreement with the other results in this thesis.

Bibliography

[1] X. Bertin, A. De Bakker, A. Van Dongeren, G. Coco, G. Andre, F. Ardhuin, P. Bonneton, F. Bouchette, B. Castelle, W. C. Crawford, et al. Infragravity waves: From driving mechanisms to impacts. *Earth-Science Reviews*, 177:774–799, 2018.

[2] M. Bjørnestad, M. Buckley, H. Kalisch, M. Streßer, J. Horstmann, H. G. Frøysa, O. E. Ige, M. Cysewski, and R. Carrasco-Alvarez. Lagrangian measurements of orbital velocities in the surf zone. *Submitted*, 2021.

[3] H. Borluk and H. Kalisch. Particle dynamics in the kdv approximation. *Wave Motion*, 49(8):691–709, 2012.

[4] A. Bowen, D. Inman, and V. Simmons. Wave 'set-down'and set-up. *Journal of Geophysical Research*, 73(8):2569–2577, 1968.

[5] M. K. Brun and H. Kalisch. Convective wave breaking in the kdv equation. *Analysis and Mathematical Physics*, 8(1):57–75, 2018.

[6] M. L. Buckley, R. J. Lowe, J. E. Hansen, A. R. van Dongeren, and C. D. Storlazzi. Mechanisms of wave-driven water level variability on reef-fringed coastlines. *Journal of Geophysical Research: Oceans*, 123(5):3811–3831, 2018.

[7] Y.-Y. Chen, H.-C. Hsu, and G.-Y. Chen. Lagrangian experiment and solution for irrotational finite-amplitude progressive gravity waves at uniform depth. *Fluid Dynamics Research*, 42(4):045511, 2010.

[8] M. W. Dingemans. *Water wave propagation over uneven bottoms*, volume 13. World Scientific, 1997.

[9] J. Grue and J. Kolaas. Experimental particle paths and drift velocity in steep waves at finite water depth. *Journal of Fluid Mechanics*, 810(R1):1–10, 2017.

[10] Z. Khorsand and H. Kalisch. On the shoaling of solitary waves in the kdv equation. *Coastal Engineering Proceedings*, (34):44–44, 2014.

[11] P. K. Kundu, I. M. Cohen, and D. Dowling. Fluid mechanics 6th, 2016.

[12] M. S. Longuet-Higgins and R. Stewart. Radiation stress and mass transport in gravity waves, with application to 'surf beats'. *Journal of Fluid Mechanics*, 13(4):481–504, 1962.

[13] M. S. Longuet-Higgins and R. Stewart. Radiation stresses in water waves; a physical discussion, with applications. In *Deep sea research and oceanographic abstracts*, volume 11, pages 529–562. Elsevier, 1964.

[14] C. C. Mei. *The applied dynamics of ocean surface waves*, volume 1. World scientific, 1989.

[15] D. S. Moore, G. P. McCabe, and B. A. Craig. *Introduction to the Practice of Statistics*. Macmillan, 2017.

[16] W. Munk. Surf beats. *EOS, Transactions American Geophysical Union*, 30(6):849–854, 1949.

[17] M. O. Paulsen and H. Kalisch. A nonlinear formulation of radiation stress and applications to cnoidal shoaling. *arXiv preprint arXiv:2102.12176*, 2021.

[18] I. Svendsen and O. Brink-Kjaer. Shoaling of cnoidal waves. In *Coastal Engineering 1972*, pages 365–383. 1973.

[19] R. E. Thomson and W. J. Emery. *Data analysis methods in physical oceanography*. Newnes, 2014.

[20] M. Tucker. Surf beats: Sea waves of 1 to 5 min. period. *Proceedings of the Royal Society of London. Series A. Mathematical and Physical Sciences*, 202(1071):565–573, 1950.

[21] T. Van Den Bremer and Ø. Breivik. Stokes drift. *Philosophical Transactions of the Royal Society A: Mathematical, Physical and Engineering Sciences*, 376(2111):20170104, 2018.

[22] T. Van den Bremer and P. H. Taylor. Lagrangian transport for two-dimensional deep-water surface gravity wave groups. *Proceedings of the Royal Society A: Mathematical, Physical and Engineering Sciences*, 472(2192):20160159, 2016.

[23] G. B. Whitham. *Linear and nonlinear waves*. John Wiley & Sons, 1974.